

# Local Projection Inference in High Dimensions

Robert Adamek<sup>†</sup>, Stephan Smeekes<sup>‡</sup>, Ines Wilms<sup>‡</sup>

<sup>†</sup>Department of Economics and Business Economics, Aarhus University,  
Fuglesangs Allé 4, 8210 Aarhus V, Denmark

Email: `r.adamek@econ.au.dk`

<sup>‡</sup>Department of Quantitative Economics, Maastricht University,  
Tongersestraat 53, 6211LM, The Netherlands

Email: `{s.smeekes,i.wilms}@maastrichtuniversity.nl`

April 18, 2024

## Abstract

In this paper, we estimate impulse responses by local projections in high-dimensional settings. We use the desparsified (de-biased) lasso to estimate the high-dimensional local projections, while leaving the impulse response parameter of interest unpenalized. We establish the uniform asymptotic normality of the proposed estimator under general conditions. Finally, we demonstrate small sample performance through a simulation study and consider two canonical applications in macroeconomic research on monetary policy and government spending.

**Keywords:** Local projections, Impulse response analysis, High-dimensional data, Honest inference, Lasso

## 1 Introduction

In this paper, we develop a simple approach for conducting valid inference on impulse responses in high-dimensional settings. We do so by pairing the estimation framework of local projections (LPs) with the inference framework of the desparsified (or debiased) lasso. Since their introduction by Jordà (2005), LPs have been widely used in macroeconomic research for studying the dynamic propagation of shocks through impulse response analysis, see e.g. Angrist et al. (2018), Ramey and Zubairy (2018), Ramey (2016) and Stock and Watson (2018). As such, they have become an increasingly used alternative to structural Vector AutoRegressions (SVAR) pioneered by Sims (1980), see for instance Ramey (2016) or Kilian and Lütkepohl (2017) for an overview on this work.

While the methods have different finite-sample properties, SVARs and LPs are equivalent in population, as established by Plagborg-Møller and Wolf (2021) who show that the underlying impulse response estimands are the same for both. This implies that the well-documented necessity for SVARs to add assumptions in order to achieve structural identification of the impulse responses, is equally true for LPs. Indeed, Plagborg-Møller and Wolf (2021) show that the identification strategies typically used for SVARs have an equivalent implementation for LPs, and vice versa. While identification issues therefore do not affect the choice between SVAR or LP, finite-sample

considerations about estimation and inference problem do. LP impulse responses are obtained by estimating only univariate linear regressions, and performing standard inference on (typically) a single parameter of interest across these univariate regressions. In contrast, SVARs require estimating the whole system of equations, and transforming these into the Vector Moving Average (VMA) representation from which the impulse responses can be derived. While the system estimation of the SVAR can still be done linearly, the inversion to the VMA representation is a nonlinear operation that renders the impulse response coefficients a complex nonlinear functions of *all* VAR parameters. This makes inference considerably more cumbersome, even in low-dimensional settings, where the complications and inaccuracies of applying the Delta method in finite samples have led to bootstrap inference becoming the norm (see e.g. Chapter 12 of Kilian and Lütkepohl, 2017, and the references therein). These problems are exacerbated when the dimensionality of the system grows, making LPs our method of choice to obtain impulse responses in high dimensions.

We consider high-dimensional local projections (HDLPs) in a general time series framework where the number of regressors can grow faster than the sample size. Impulse response analysis quickly becomes high-dimensional in macroeconomic research. Even when considering impulse response analysis with few variables, the number of regressors in LPs or SVARs is often large due to the common practices of including many lags to control for autocorrelation (see e.g., Bernanke and Mihov, 1998, Romer and Romer, 2004 and Sims and Zha, 2006) or to robustify against (near) unit roots via lag augmentation as in Montiel Olea and Plagborg-Møller (2021). Similarly, additional regressors are often introduced to capture seasonal patterns in impulse responses (see e.g., quarter-dependent coefficients used in Blanchard and Perotti, 2002), or to permit nonlinearities to produce state-dependent impulse responses (Koop et al., 1996; Ramey and Zubairy, 2018).

Additionally, one might be interested in impulse response analysis with many variables. Motivations of the latter include, amongst others, avoidance of contaminated measurements of policy innovations or informational deficiency with impulse response estimates that are distorted by omitted variable bias, the ability to use several observable measures of difficult-to-measure variables in theoretical models, or opportunities for researchers and policy makers to investigate the impact of shocks on a larger, possibly more disaggregated set of variables they care about (see e.g., Bernanke et al., 2005, Forni and Gambetti, 2014, Stock and Watson, 2016 and Kilian and Lütkepohl, 2017, Ch. 16).

Regular estimation approaches, however, become infeasible for high-dimensional settings. Traditional approaches to high-dimensionality include modelling commonalities between variables, such as through factor-augmented VARs (FAVAR) (Bernanke et al., 2005), dynamic factor models (DFM) (Forni et al., 2009; Stock and Watson, 2016) or – for panel structures – global VARs (Chudik and Pesaran, 2016); as well as Bayesian shrinkage methods (Bańbura et al., 2010; Chan, 2020). Recently, sparse shrinkage methods such as the lasso have gained considerable popularity in econometrics for policy evaluation (Belloni et al., 2014) and (macroeconomic) time series analysis (Kock et al., 2020). Their use in impulse response analysis however has only scarcely been explored.

While several methods and theoretical results now exist for estimating sparse VAR models – see e.g., Basu and Michailidis (2015); Kock and Callot (2015); Masini et al. (2022) and the references cited therein – inference on impulse responses is complicated by two issues. First, sparse estimation techniques such as the lasso perform model selection, which induces issues with non-uniformity of limit results if this selection is ignored (Leeb and Pötscher, 2005). Second, while several methods such as orthogonalization (Belloni et al., 2014) and debiasing, or desparsifying the lasso (van de

Geer et al., 2014; Javanmard and Montanari, 2014) have been proposed to yield uniformly valid (or ‘honest’) post-selection inference, the impulse response parameters are nonlinear functions of all estimated VAR parameters. This severely limits the applicability of existing post-selection inference methods which are typically designed for (relatively) low-dimensional parameters of interest that can be estimated directly. Indeed, to our knowledge, impulse response analysis in sparse HD-SVARs is only considered in Krampe et al. (2022), who construct a complex multi-step algorithm to overcome these complications. Instead, by casting the problem in the LP framework, we reduce the impulse response parameter(s) to a (directly estimable) low-dimensional object in the presence of high-dimensional nuisance parameters, which makes the standard post-selection tools available.

We develop HDLP inference based on the desparsified lasso of van de Geer et al. (2014) and its time series extension in Adamek et al. (2022b). The latter has recently been empirically investigated in the context of LP estimation with instrumental variables (LP-IV) in contemporaneous work by Karapanagioti (2021). Their approach not only differs in the focus on IV models, but they also apply the method of Adamek et al. (2022b) ‘as is’. Instead, we tailor the approach of Adamek et al. (2022b) specifically to high-dimensional LPs consisting of a small number of parameters of interest – the dynamic response of a variable to a shock at a given horizon – and many controls. In particular, we modify their approach by leaving the parameter of interest unpenalized during the estimation procedure to ensure it does not suffer from penalization bias. Such a setting is of more general relevance for treatment effect models consisting of a small number of variables whose effects are of interest combined with a large set of controls. We theoretically show that the combination of few unpenalized parameters with many penalized ones does not affect the asymptotic behaviour of the desparsified lasso.

Through simulation experiments, we show that our proposed estimator has considerably better coverage rates than the standard desparsified lasso in finite samples. Furthermore, on an empirically calibrated DFM (Li et al., 2021) we find that our proposed HDLP method shows competitive performance in a sparse DFM compared to a low-dimensional LP and a factor-augmented LP.

We consider two canonical macroeconomic applications and demonstrate the performance of the proposed desparsified-lasso based estimator for HDLPs in recovering structural impulse responses. Specifically, we first extend the work of Bernanke et al. (2005) on macroeconomic responses to a shock in monetary policy to a HDLP setting. Second, we consider the work by Ramey and Zubairy (2018) on state-dependent impulse responses to a shock in government spending, as also studied by Karapanagioti (2021) in their LP-IV setting, but we extend the original specification used in Ramey and Zubairy (2018) to a HDLP specification with more lags as well as a more complex state-dependent HDLP with interaction between different state variables. The methods needed for these applications are implemented in the R package `desla` (Adamek et al., 2022a), which also offers the methods of Adamek et al. (2022b).

The paper is organized as follows. Section 2 introduces the model and our inferential procedure, as well as our main result on the asymptotic normality of the desparsified lasso. Section 3 contains simulation studies that examine the small sample performance of the proposed desparsified lasso. Section 4 presents the results of the two macroeconomic applications. Section 5 concludes.

A word on notation. For any  $N$  dimensional vector  $\mathbf{x}$ ,  $\|\mathbf{x}\|_r = \left(\sum_{i=1}^N |x_i|^r\right)^{1/r}$  denotes the  $l_r$ -norm, with the convention that  $\|\mathbf{x}\|_0 = \sum_i 1(|x_i| > 0)$ . Depending on the context,  $\sim$  denotes equivalence in order of magnitude of sequences, or equivalence in distribution.

## 2 High-dimensional Local Projections

Consider the local projection regression

$$y_{t+h} = \phi_h x_t + \rho_h y_t + \boldsymbol{\eta}'_h \mathbf{w}_{s,t} + \sum_{k=1}^K \boldsymbol{\delta}'_{h,k} \mathbf{z}_{t-k} + u_{h,t}, \quad h = 0, 1, \dots, h_{\max}, \quad (2.1)$$

where  $\phi_h, \rho_h, \boldsymbol{\eta}_h, \boldsymbol{\delta}_{h,k}$  are the projection parameters,  $u_{h,t}$  is the projection error and the set of variables  $\mathbf{z}_t = (\mathbf{w}'_{s,t}, y_t, x_t, \mathbf{w}'_{f,t})'$  consist of the response  $y_t$ , the shock variable  $x_t$ , and the vectors of control variables split into the “slow” variables  $\mathbf{w}_{s,t} \in \mathbb{R}^{n_s}$ , and the “fast” ones  $\mathbf{w}_{f,t} \in \mathbb{R}^{n_f}$  for identification purposes, as discussed below.<sup>1</sup> Our single parameter of interest is  $\phi_h$ , the dynamic response at horizon  $h$  of  $y_t$  after an impulse in  $x_t$ . The LP impulse response function of  $y_t$  with respect to  $x_t$  is given by  $\{\phi_h\}_{h \geq 0}$  and can be obtained by estimating eq. (2.1) for  $h = 0, 1, \dots, h_{\max}$ .

To permit causal interpretation of the impulse responses, structural assumptions about the data generating process are needed. Example 2.1 considers a Structural Vector Moving Average model (see Assumption 3 in Plagborg-Møller and Wolf, 2021) as an example.

**Example 2.1** (SVMA). Consider the Structural Vector Moving Average (SVMA)

$$\mathbf{z}_t = \boldsymbol{\mu} + \mathbf{A}(L)\boldsymbol{\epsilon}_t, \quad \mathbf{A}(L) = \sum_{k=0}^{\infty} \mathbf{A}_k L^k, \quad \boldsymbol{\epsilon}_t \stackrel{i.i.d.}{\sim} N(\mathbf{0}, \mathbf{I}), \quad (2.2)$$

where  $\boldsymbol{\epsilon}_t$  is a vector of structural shocks,  $L$  is the lag operator,  $\{\mathbf{A}_k\}_k$  is absolutely summable, and  $\mathbf{A}(x)$  has full row rank for all complex scalars  $x$  on the unit circle.

While an assumption such as Example 2.1 is necessary to recover the structural impulse responses, it is not a sufficient condition:  $\mathbf{A}_0$  is not identified without further restrictions. We focus on impulse responses identified by a (partially) recursive structure. This can be implemented in LPs by partitioning the variables in  $\mathbf{z}_t$  into slow variables ( $\mathbf{w}_{s,t}$ ) and fast variables ( $\mathbf{w}_{f,t}$ ). The slow variables are predetermined with respect to  $x_t$ , while the fast variables can react contemporaneously to the shock variable  $x_t$  and therefore only enter the equation with a lag. Equivalently, in the language of recursively identified SVARs,  $\mathbf{w}_{s,t}$  is ordered above  $x_t$ , while  $\mathbf{w}_{f,t}$  is ordered below. Note also that in eq. (2.1) we assume that  $y_t$  is predetermined with respect to (ordered above)  $x_t$ ; if the reverse were true one should remove  $y_t$  from the right-hand side of eq. (2.1).<sup>2</sup>

Equation (2.1) can also be used outside of the recursive identification framework, for example when the structural shock is externally identified. Examples of the latter are the narrative monetary policy shock series of Romer and Romer (2004), or the military spending series of Ramey and Zubairy (2018). One can then directly take  $x_t = \epsilon_{1,t}$  provided the structural shock is observed without measurement error. Given the exogeneity (and thus predeterminedness) of such shocks, all other variables would then be considered to be “fast” and no variable would be included contemporaneously; see e.g. Example 2.2.

Section 3.2 of Plagborg-Møller and Wolf (2021) provides detailed discussions on how other identification schemes, such as sign restrictions, can be imposed while estimating eq. (2.1); these arguments generally remain valid in our high-dimensional setup as well. However, identification through instrumental variables as in e.g. Stock and Watson (2018) becomes more complicated.

<sup>1</sup>We omit the constant, since we generally demean the data when using the desparsified lasso.

<sup>2</sup>In this situation, the model would be equivalent to equation (1) of Plagborg-Møller and Wolf (2021).

Adapting IV estimation methods such as two-stage least-squares (Plagborg-Møller and Wolf, 2021, Section 3.3) to high dimensions requires a different setup for the desparsified lasso (see e.g. Gold et al., 2020), which has not yet been explored for time series models. This remains an interesting avenue for future research.

While the LP in eq. (2.1) has a single parameter of interest, it can easily be extended to allow for LPs with a small number of parameters of interest, see Example 2.2.

**Example 2.2** (State-Dependent LP). Consider the nonlinear state-dependent model of Ramey and Zubairy (2018):

$$y_{t+h} = I_{t-1} \left[ \alpha_h + \phi_{A,h} x_t + \sum_{k=1}^K \delta'_{A,h,k} z_{t-k} \right] + (1 - I_{t-1}) \left[ \phi_{B,h} x_t + \sum_{k=1}^K \delta'_{B,h,k} z_{t-k} \right] + u_{h,t}. \quad (2.3)$$

Here,  $\phi_{A,h}$  and  $\phi_{B,h}$  are the two responses of  $y_t$  after an impulse in  $x_t$ , corresponding to two different states distinguished by the dummy variable  $I_t$ .

To generally accommodate LP settings with a small number of parameters of interest and a large number of controls, we will use the more general notation

$$y_t = \mathbf{x}'_{\mathcal{H},t} \boldsymbol{\beta}_{\mathcal{H}} + \mathbf{x}'_{-\mathcal{H},t} \boldsymbol{\beta}_{-\mathcal{H}} + u_t, \quad t = 1, \dots, T, \quad (2.4)$$

$1 \times H \quad H \times 1 \quad 1 \times (N-H) \quad (N-H) \times 1$

and in matrix form

$$\mathbf{y} = \mathbf{X}_{\mathcal{H}} \boldsymbol{\beta}_{\mathcal{H}} + \mathbf{X}_{-\mathcal{H}} \boldsymbol{\beta}_{-\mathcal{H}} + \mathbf{u}.$$

We hereby separate the parameter vector  $\boldsymbol{\beta} = [\boldsymbol{\beta}'_{\mathcal{H}}, \boldsymbol{\beta}'_{-\mathcal{H}}]'$  into two groups. The first group consists of the  $H$ -dimensional set of parameters of interest  $\boldsymbol{\beta}_{\mathcal{H}}$ , corresponding to the variables  $\mathbf{x}_{\mathcal{H},t}$ , which will be unpenalized during the estimation procedure to ensure they are not affected by penalization bias. The second group consists of the large set of parameters  $\boldsymbol{\beta}_{-\mathcal{H}}$ , corresponding to control variables  $\mathbf{x}_{-\mathcal{H},t}$ , which will be penalized during the estimation procedure. We hereby use  $\mathcal{H}$  to denote the set that indexes the  $H$  variables of interest. Without loss of generality, we order these variables first in  $\mathbf{X} = [\mathbf{X}_{\mathcal{H}}, \mathbf{X}_{-\mathcal{H}}]$ . Finally, since each horizon  $h$  of the LPs is estimated separately, we suppress the dependence on  $h$  in our notation.

## 2.1 Local Projection Estimation

We start by estimating eq. (2.4) with the lasso to obtain an initial estimate of  $\boldsymbol{\beta}$ , while leaving the parameters of interest  $\boldsymbol{\beta}_{\mathcal{H}}$  unpenalized. The first stage lasso is defined as

$$\hat{\boldsymbol{\beta}}^{(L)} = [\hat{\boldsymbol{\beta}}^{(L)'}_{\mathcal{H}}, \hat{\boldsymbol{\beta}}^{(L)'}_{-\mathcal{H}}]' = \arg \min_{\boldsymbol{\beta}^* \in \mathbb{R}^N} \|\mathbf{y} - \mathbf{X} \boldsymbol{\beta}^*\|_2^2 / T + 2\lambda \|\mathbf{W} \boldsymbol{\beta}^*\|_1, \quad (2.5)$$

where  $\mathbf{W}$  is an  $N \times N$  diagonal matrix with  $\mathbf{W}_{i,i} = 0$  for  $i \in \mathcal{H}$  and 1 otherwise. The Frish-Waugh-Lovell-style result of Yamada (2017) ensures that the penalized and unpenalized estimates can be respectively obtained by

$$\begin{aligned} \hat{\boldsymbol{\beta}}^{(L)}_{-\mathcal{H}} &= \arg \min_{\boldsymbol{\beta}^* \in \mathbb{R}^{(N-H)}} \|\mathbf{M}(\mathbf{X}_{\mathcal{H}}) \mathbf{y} - \mathbf{M}(\mathbf{X}_{\mathcal{H}}) \mathbf{X}_{-\mathcal{H}} \boldsymbol{\beta}^*\|_2^2 / T + 2\lambda \|\boldsymbol{\beta}^*\|_1, \\ \hat{\boldsymbol{\beta}}^{(L)}_{\mathcal{H}} &= \hat{\boldsymbol{\Sigma}}_{\mathcal{H}}^{-1} \mathbf{X}'_{\mathcal{H}} (\mathbf{y} - \mathbf{X}_{-\mathcal{H}} \hat{\boldsymbol{\beta}}^{(L)}_{-\mathcal{H}}) / T, \end{aligned}$$

where the residual maker  $\mathbf{M}_{(\mathbf{X}_{\mathcal{H}})} := (I - \mathbf{X}_{\mathcal{H}}(\mathbf{X}'_{\mathcal{H}}\mathbf{X}_{\mathcal{H}})^{-1}\mathbf{X}'_{\mathcal{H}})$ , and  $\hat{\Sigma}_{\mathcal{H}} := \frac{\mathbf{X}'_{\mathcal{H}}\mathbf{X}_{\mathcal{H}}}{T}$ . We can therefore use regular lasso estimation on the transformed response  $\mathbf{M}_{(\mathbf{X}_{\mathcal{H}})}\mathbf{y}$  and predictors  $\mathbf{M}_{(\mathbf{X}_{\mathcal{H}})}\mathbf{X}_{-\mathcal{H}}$  to obtain  $\hat{\beta}_{-\mathcal{H}}^{(L)}$ .

We next “desparsify” this estimate to allow for uniformly valid inference. The desparsified lasso estimator is defined as

$$\hat{\beta}_{\mathcal{H}} := \hat{\beta}_{\mathcal{H}}^{(L)} + \hat{\Theta}\mathbf{X}'(\mathbf{y} - \mathbf{X}\hat{\beta}^{(L)})/T, \quad (2.6)$$

where  $\hat{\Theta}$  is an  $H \times N$  submatrix of an approximate inverse of  $\hat{\Sigma} := \frac{\mathbf{X}'\mathbf{X}}{T}$ . We obtain  $\hat{\Theta}$  from ‘nodewise’ regressions, which estimate the linear projections of  $\mathbf{x}_j$  onto  $\mathbf{X}_{-j}$ , where  $\mathbf{x}_j$  is the  $j$ th column of  $\mathbf{X}$  and  $\mathbf{X}_{-j}$  is  $\mathbf{X}$  without the  $j$ th column. We let

$$\hat{\gamma}_j = \arg \min_{\gamma_j^* \in \mathbb{R}^{N-1}} \|\mathbf{x}_j - \mathbf{X}_{-j}\gamma_j^*\|_2^2/T + 2\lambda_j \|\gamma_j^*\|_1,$$

and construct  $\hat{\Theta} := \hat{\Upsilon}^{-2}\hat{\Gamma}$ , where  $\hat{\Upsilon}^{-2} := \text{diag}(1/\hat{\tau}_1^2, \dots, 1/\hat{\tau}_H^2)$ , with  $\hat{\tau}_j^2 = \|\hat{\mathbf{v}}_j\|_2^2/T + \lambda_j \|\hat{\gamma}_j\|_1$ ,  $\hat{\mathbf{v}}_j = \mathbf{x} - \mathbf{X}\hat{\gamma}_j$  and  $\hat{\Gamma}$  stacks the  $\hat{\gamma}_j$ ’s row-wise:

$$\hat{\Gamma} := \begin{bmatrix} 1 & \dots & -\hat{\gamma}_{1,H} & \dots & -\hat{\gamma}_{1,N} \\ \vdots & \ddots & \vdots & & \vdots \\ -\hat{\gamma}_{H,1} & \dots & 1 & \dots & -\hat{\gamma}_{H,N} \end{bmatrix}.$$

The specific structure of the LPs consisting of the same set of regressors at each horizon  $h$  allows for computational and efficiency gains in obtaining the desparsified lasso. The initial lasso in eq. (2.5) should be obtained for each horizon, but the population linear projection coefficients  $\gamma_j$  in the nodewise regression do not change with the horizon. It is therefore sufficient to compute the nodewise lasso estimator once. This can be done best at horizon zero where most time points are available for estimating the nodewise regression. We therefore partly avoid the loss of efficiency at further horizons where the most recent observation at each new horizon would be lost for estimation otherwise. As an example, for the LP in eq. (2.1), we estimate

$$x_t = \psi'_0(y_t, \mathbf{w}'_{s,t})' + \sum_{k=1}^K \psi'_k \mathbf{z}_{t-k} + v_{1,t}, \quad (2.7)$$

then store  $\hat{\Theta}$  constructed from  $\hat{\gamma}_1 = [\hat{\psi}'_0, \dots, \hat{\psi}'_K]'$ , and the residual vector  $\hat{\mathbf{v}}_1$ . The former can then be re-used at each horizon in the desparsified lasso estimator in eq. (2.6), while the latter can be re-used in the estimation of the long-run covariance matrix which enters the asymptotic distribution of the desparsified lasso, see Section 2.2.

Finally, regarding the choice of tuning parameter  $\lambda$  in the initial regression and  $\lambda_j$  in the nodewise regressions, we follow the approach of Adamek et al. (2022b) who propose an iterative plug-in procedure that simulates the quantiles of an appropriate “empirical process” which should be dominated by  $\lambda$ ; see their Section 5.1 for details.

## 2.2 Local Projection Inference

We next discuss the asymptotic properties of  $\hat{\beta}_{\mathcal{H}}$ . The assumptions needed for our analysis are listed in detail in Appendix A, and are discussed briefly below. Detailed discussions can be found

in Adamek et al. (2022b), on whose approach our theory is built.

We need assumptions on the DGP (Assumption A.1), the sparsity of the parameter (A.2), regularity conditions for high-dimensional settings (A.3) and assumptions on the set of parameters on which inference is conducted (A.4). Assumption A.1(a) requires that the regressors are contemporaneously uncorrelated with the error term, and that the error terms and the variables in  $\mathbf{z}_t$  have finite unconditional moments up to a certain order. Crucially, Assumption A.1(a) allows for serial correlation in the error terms, which is a typical feature of LP regressions. Assumption A.1(c) assumes  $\mathbf{z}_t$  to be near-epoch-dependent (NED). An NED process can be interpreted as a process that is well-approximated by a mixing process, but does not have to be mixing itself. Unlike mixing conditions, which may exclude even very simple autoregressive processes, NED conditions permit very general forms of dependence often encountered in macroeconomic research, see Adamek et al. (2022b) for a more detailed discussion.

Comparing our DGP assumptions to the SVMA assumptions of Example 2.1, one can verify that the moment condition is satisfied trivially under Gaussianity, and the NED assumption can be shown to hold when the VMA coefficients  $\mathbf{A}_k$  converge to 0 sufficiently quickly; see Example 17.3 of Davidson (2002). If one would relax the Gaussianity assumption, a trade-off would occur between the number of moments and the allowed dependence – the more moments, the more persistent the process may be.

Second, we impose a sparsity assumption on the parameter  $\boldsymbol{\beta}$  (Assumption A.2), as typically required for lasso estimators. We derive our results under weak sparsity, thereby recognizing that the true parameters are likely not exactly zero. In particular, we assume that  $\|\boldsymbol{\beta}\|_r^r$  is sufficiently small for some  $0 \leq r < 1$ . While for  $r = 0$  our results boil down to requiring exact sparsity for larger values of  $r$ , we allow for many non-zero entries in  $\boldsymbol{\beta}$  provided they are relatively small. The smaller  $r$ , the more restrictive this assumption therefore is. We also require weak sparsity in the nodewise regressions, which amounts to assuming that the inverse population covariance matrix  $\boldsymbol{\Sigma}^{-1} := (\mathbb{E}\mathbf{X}'\mathbf{X}/T)^{-1}$  is sparse in (induced)  $r$ -norm. Since eq. (2.1) has a similar regressor structure as a VAR, this can be shown to hold under conditions similar to the sparse VAR in Example 6 of Adamek et al. (2022b).

Next, we require that the minimum eigenvalue of  $\boldsymbol{\Sigma}$  is bounded away from 0 (Assumption A.3). This assumption ensures that the population covariance matrix of the regressors remains well-behaved with increasing  $N$ . Again, thanks to the similarity of eq. (2.1) to a VAR, lower bounds on the minimum eigenvalue can be derived using the results on page 6 of Masini et al. (2022). Finally, we also require that the number of unpenalized parameters of interest to be bounded (Assumption A.4). In LPs, this is trivially satisfied, for instance  $H = 1$  in eq. (2.1), and  $H = 3$  in eq. (2.3).<sup>3</sup>

Under these assumptions, Theorem 2.1 establishes the asymptotic normality of our desparsified lasso estimator, which allows for valid asymptotic inference.

**Theorem 2.1.** *Under Assumptions A.1 to A.5, for the model in eq. (2.4), we have*

$$\sup_{\substack{\boldsymbol{\beta} \in \mathbf{B}_N(r, s_r) \\ z \in \mathbb{R}}} \left| \mathbb{P} \left( \sqrt{T} \frac{\mathbf{r}'(\hat{\boldsymbol{\beta}}_{\mathcal{H}} - \boldsymbol{\beta}_{\mathcal{H}})}{\sqrt{\mathbf{r}'\hat{\boldsymbol{\Upsilon}}^{-2}\hat{\boldsymbol{\Omega}}\hat{\boldsymbol{\Upsilon}}^{-2}\mathbf{r}}} \leq z \right) - \Phi(z) \right| = o_p(1),$$

---

<sup>3</sup>While the impulse responses are the two parameters of interest, we may also want to leave the dummy parameter unpenalized.

where  $\Phi(\cdot)$  is the CDF of  $N(0, 1)$ ,  $\mathbf{r} \in \mathbb{R}^{\mathcal{H}}$  is chosen to test hypotheses of the form  $\mathbf{r}'\boldsymbol{\beta}_H = 0$ , and  $\hat{\boldsymbol{\Omega}}$  is a consistent long-run covariance estimator.

Note that in LPs, the errors  $u_{h,t}$  from eq. (2.1) are generally autocorrelated due to the leads of  $y_t$  on the left-hand side. As in Adamek et al. (2022b), we therefore use an autocorrelation robust Newey-West long-run covariance estimator  $\hat{\boldsymbol{\Omega}} := \sum_{l=1-Q_T}^{Q_T-1} (1 - l/Q_T) \hat{\boldsymbol{\Xi}}(l)$ , with bandwidth  $Q_T < T$ , where  $\hat{\boldsymbol{\Xi}}(l) := \frac{1}{T-l} \sum_{t=l+1}^T \hat{\mathbf{q}}_t \hat{\mathbf{q}}_{t-l}'$ ,  $\hat{\mathbf{q}}_t := (\hat{v}_{1,t}, \dots, \hat{v}_{H,t})' \hat{u}_t$ . To obtain our asymptotic results, we generally require that the bandwidth  $Q_T$  grows as  $T \rightarrow \infty$  at a sufficiently slow rate, see Assumption A.5 in Appendix A for details. Regarding the choice of  $Q_T$  in finite samples, we use the bandwidth estimator of Andrews (1991).

For the LP in eq. (2.1), Theorem 2.1 permits asymptotic confidence intervals  $CI_h(\alpha) := \left[ \hat{\phi}_h \pm z_{\alpha/2} \sqrt{T^{-1} \hat{\omega}_h \hat{\tau}_h^{-4}} \right]$ , where  $\hat{\omega}_h$  and  $\hat{\tau}_h^{-2}$  are the scalar versions of  $\hat{\boldsymbol{\Omega}}_h$  and  $\hat{\boldsymbol{\Upsilon}}_h^{-2}$  respectively, and  $z_{\alpha/2} := \Phi^{-1}(1 - \alpha/2)$ . Note the dependence on  $h$  in this result, since the residuals  $\hat{\mathbf{u}} = \hat{\mathbf{u}}_h$  are different at each horizon, and  $\hat{\boldsymbol{\Omega}} = \hat{\boldsymbol{\Omega}}_h$  and  $\hat{\boldsymbol{\Upsilon}}^{-2} = \hat{\boldsymbol{\Upsilon}}_h^{-2}$  as well.

### 3 Simulations

We perform a simulation study to analyse the finite sample performance of the desparsified lasso estimator. In section 3.1 we compare our proposed method with unpenalized parameter of interest to the standard desparsified lasso in a sparse structural VAR. In section 3.2, we study our proposed method in an empirically calibrated DFM.

#### 3.1 Sparse Structural VAR Model

Consider the structural VAR with structural shocks  $\boldsymbol{\epsilon}_t$

$$\begin{pmatrix} y_t \\ \mathbf{w}_{s,t} \end{pmatrix} = \mathbf{z}_t = \sum_{k=1}^4 \mathbf{A}_k \mathbf{z}_{t-k} + \boldsymbol{\epsilon}_t, \quad \boldsymbol{\epsilon}_t \stackrel{iid}{\sim} N(\mathbf{0}, \mathbf{I}), \quad (3.8)$$

where the autoregressive parameter matrices  $\mathbf{A}_k$  are tapered Toeplitz matrices. We analyse the response of  $y_t$  to the first shock  $\epsilon_{1,t}$  and investigate the coverage and width of 95% point-wise confidence intervals corresponding to the impulse response parameters at horizons 1 to 10. We consider different values for the number of variables  $P = \{20, 40, 100\}$  and time series length  $T = \{100, 200, 500\}$  and report results for 1000 replications. Details on the DGP and implementation of the HDLP are included in Appendix C.1.1.

Figure 1 presents the coverage rates for the proposed desparsified lasso (blue), which leaves the impulse response parameters of interest unpenalized, in comparison to the standard desparsified lasso (red). We only display results for  $P = 40$ , but the results for  $P = 20$  and  $P = 100$  are very similar and included in Figure C.1 in Appendix C.1, alongside the interval widths in Figure C.2.

Our proposed estimator attains good coverage rates close to the nominal level of 95% for all combinations of  $P$  and  $T$ . For both DGPs, coverage rates are usually the lowest around 70-90% for horizon 1, but revert to the nominal level for larger horizons. Good coverage at further horizons is to be expected, since the local projection coefficients will tend to become more sparse in stationary models. Importantly, considerable gains are obtained compared to the standard desparsified lasso. Especially at shorter horizons – which are usually of most interest in practice – coverage rates of



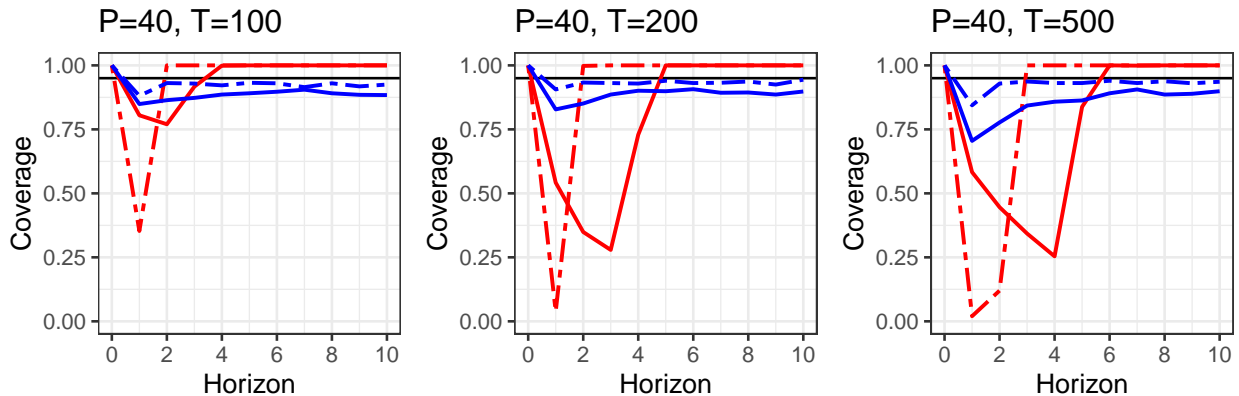


Figure 1: Coverage rates of the standard desparsified lasso (red) and the proposed desparsified lasso with  $\phi_h$  unpenalized (blue). Dashed lines indicate results for the second DGP.

the latter drop to 25% in the first DGP and even more in the second. We also see in Figure C.2 (Appendix C.1) that the interval widths are broadly similar or even smaller than the ones for the standard desparsified lasso, meaning we obtain better coverage without losing power.

The poor coverage rates of the standard desparsified lasso occur since the parameters of interest are not selected in the initial lasso regression. A simple alteration of the desparsified lasso that leaves this parameter unpenalized thus brings the coverage rates much closer to the nominal level. Note that the standard desparsified lasso has coverage exceeding our proposed estimator at further horizons; this is because the true impulse response becomes close to zero, where the lasso’s bias towards zero is beneficial. This does not run counter to our conclusion, as we believe more uniform coverage over different parameter values is desirable.

### 3.2 Empirically Calibrated Dynamic Factor Model

We now examine the performance of our proposed estimator on an empirically calibrated dynamic factor model, inspired by Lazarus et al. (2018) and Li et al. (2021). Unlike the former works which use the quarterly dataset of Stock and Watson (2016) to fit their DFM, we use the monthly FRED-MD database (McCracken and Ng, 2016a) which we analyse in Section 4. Implementation details on the simulation set-up are in Appendix C.1.2, an overview on the variables in the FRED-MD database in Appendix C.2.

We consider both a “dense” DFM where the factor loadings are obtained using principal components and a factor VAR is estimated by OLS, and a “sparse” DFM where the loadings are obtained using the WF-SOFAR estimator of Uematsu and Yamagata (2022a) and the VAR is estimated by the lasso. The dense DFM is inherently difficult for our proposed estimator since the covariance structure of the variables is dense, whereas we assume it to be sparse in Assumption A.2, and the DGP is likely to violate the sparsity of the nodewise regression coefficients. However, bounds on the sparsity of the nodewise regressions can be obtained for sparse factor models and VARs, see Example 5 and 6 of Adamek et al. (2022b). We therefore expect better coverage properties of our proposed estimator in this setting. The WF-SOFAR estimator seems particularly appropriate to use since Uematsu and Yamagata (2022b) find evidence of a sparse factor structure in the FRED-MD data.<sup>4</sup>

<sup>4</sup>The difference in sparsity between the dense and sparse DFMs is relatively limited. For details, see Figure C.3 in Appendix C.1.2.

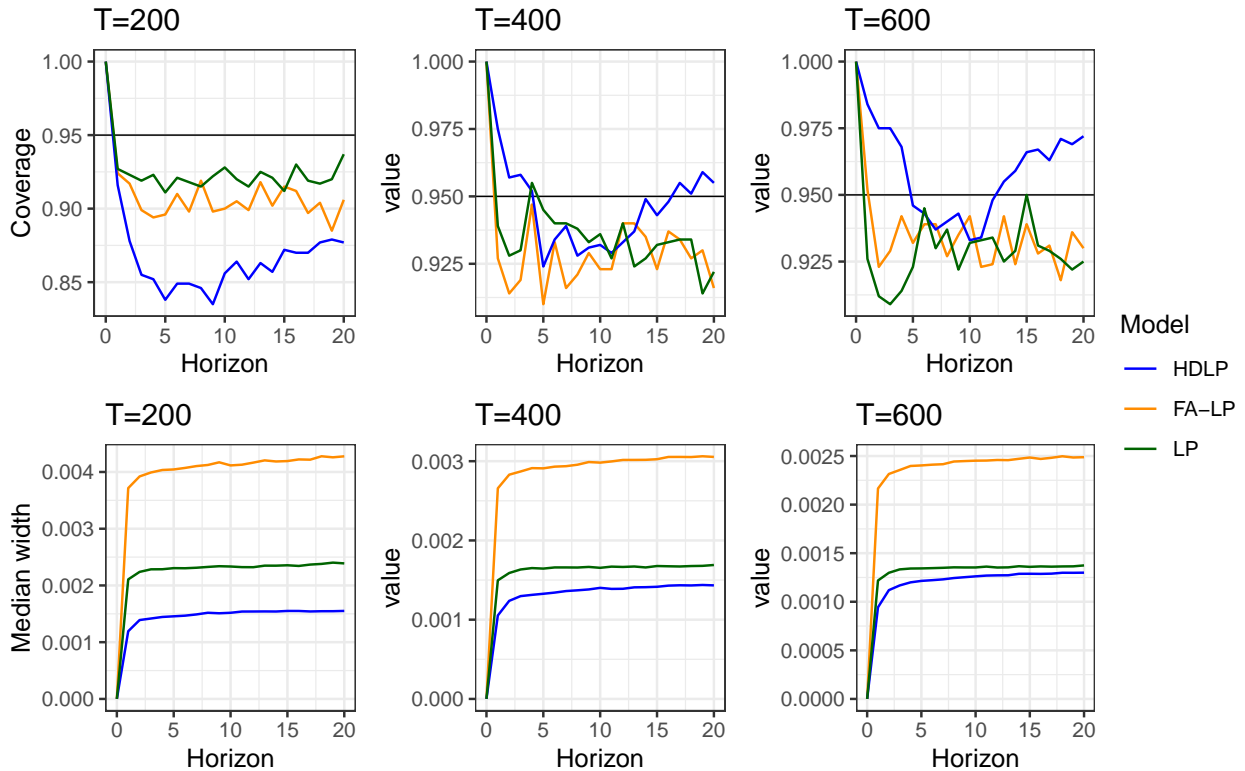


Figure 2: Coverage rates and median interval widths in the sparse DFM.

We study the impulse response of Industrial Production (IP) to the Federal Funds Rate (FFR). Our HDLP method estimates eq. (2.1) with  $y_t = IP_t$ ,  $x_t = FFR_t$ , the remaining 120 variables in  $w_{s,t}$ ,  $w_{f,t}$  empty, and 3 lags included.<sup>5</sup> We compare the performance of our proposal to two benchmarks. The first benchmark is a factor-augmented local projection, labelled “FA-LP”. We favour FA-LP by including the true number of six factors, estimated by principal components from the 120 variables, and estimate the FA-LP by OLS. As this method matches the true DGP closely, we expect this benchmark to be a highly competitive standard. Our second benchmark is a 3-variable LP (estimated by OLS) with consumer price index as third variable as in Bernanke et al. (2005). This benchmark, labelled “LP”, allows us to assess the gain in using high-dimensional data. All models are estimated using the R package `desla` (Adamek et al., 2022a), taking the plug-in constant equal to 0.4 for the HDLP.

In the dense DFM, see Figure C.4 in Appendix C, our proposed HDLP method attains coverage around 70% for the first 5 periods, then steadily improves at further horizons where it reaches nominal coverage around horizon 20 for large sample sizes. The benchmarks perform, however, considerably better as expected. They perform similarly at  $T = 200$  with 90% coverage, but diverge at larger sample sizes. The FA-LP model has improved coverage at larger samples, reaching nominal at  $T = 600$ , whereas the coverage of the LP deteriorates at larger samples.

In the sparse DFM (Figure 2), the performance of the HDLP considerably improves. Its coverage (top panels) is still below the benchmarks for  $T = 200$ , stays around 85% for all horizons, but it matches or exceeds the benchmarks at larger sample sizes. The performance of the FA-LP is similar to that of the dense DFM, and the LP benchmark maintains similar coverage to the FA-LP even at larger sample sizes; the 3-variable LP is likely a better approximation of the sparse DFM than the

<sup>5</sup>Each local projection therefore has 488 regressors.

dense DFM. Importantly though, we see across all sample sizes that the widths (bottom panels) of the FA-LP benchmark are 2-4 times larger than those of the HDLP, while the LP widths are also wider everywhere though to a lesser extent.

One should keep in mind that we set up the simulations advantageously to the FA-LP by using the true number of factors. The superior performance of the FA-LP, particularly for the dense model where our HDLP is expected to suffer, is thus hardly surprising. Yet for the sparse DFM, our HDLP method outperforms both the idealized FA-LP and the 3-variable LP with comparable or superior coverage yet considerably tighter intervals.

To conclude our simulation experiments, we investigate the sensitivity of our method to the choice of long-run covariance estimator. We compare the Newey-West (NW) estimator to the fixed- $b$  Newey-West and Equal-Weighted Cosine (EWC) estimator suggested by Lazarus et al. (2018). In Appendix C.1.3 we find that the first generally performs slightly worse than our default choice of Newey-West (likely due to our adaptive choice of bandwidth), whereas the second performs very well in terms of coverage but has confidence intervals around 4-6 times as wide as the ones from our NW estimator. In settings where our method has good coverage, such as the sparse DFM, EWC thus provides little benefit. We therefore proceed with our default choice of NW estimator in the remainder of the paper, but these alternatives are available in the `desla` package.

## 4 Structural Impulse Responses Estimated by HDLPs

We apply the desparsified lasso for HDLPs to two canonical macroeconomic applications. In Section 4.1, we build on the work by Bernanke et al. (2005) on monetary policy analysis, in Section 4.2 we build on the work by Ramey and Zubairy (2018) on government spending. All analyses are performed in R using the package `desla`.

### 4.1 Impulse Responses to a Shock in Monetary Policy

We consider the work by Bernanke et al. (2005), wherein they estimate impulse responses to a monetary policy shock identified by the federal funds rate in a factor-augmented SVAR. We use HDLPs to perform the impulse response analysis and expand the dataset of the original paper to the more recent and larger FRED-MD database (McCracken and Ng, 2016b), thereby considering monthly data from January 1960 to October 2008 for 122 macroeconomic variables. For a full description of the data, see Appendix C.2.

We estimate the HDLP in eq. (2.1), where as response variables  $y_t$  we take the federal funds rate (FFR), industrial production (IP) and the consumer price index (CPI). As shock variable of interest  $x_t$  we consider the federal funds rate (FFR). Furthermore, we use the identification strategy of Bernanke et al. (2005), which consists of classifying variables as “slow” in  $w_{s,t}$  or “fast” in  $w_{f,t}$ , according to whether these variables can respond within the same month to an unexpected change in the FFR.<sup>6</sup> For variables in FRED-MD that can be directly matched to their counterparts in the DRI/McGraw Hill Basic Economics Database, we use the same slow/fast classification as Bernanke et al. (2005). For new variables in FRED-MD, we apply the same general classification rule; i.e., variables in the categories Prices, Output & Income, Labour Market, and Consumption

---

<sup>6</sup>As discussed before, this strategy is equivalent to recursive (partial) identification in an SVAR, as shown in Example 1 of Plagborg-Møller and Wolf (2021). In fact, this application can also be seen as a high-dimensional extension of Christiano et al. (2005).

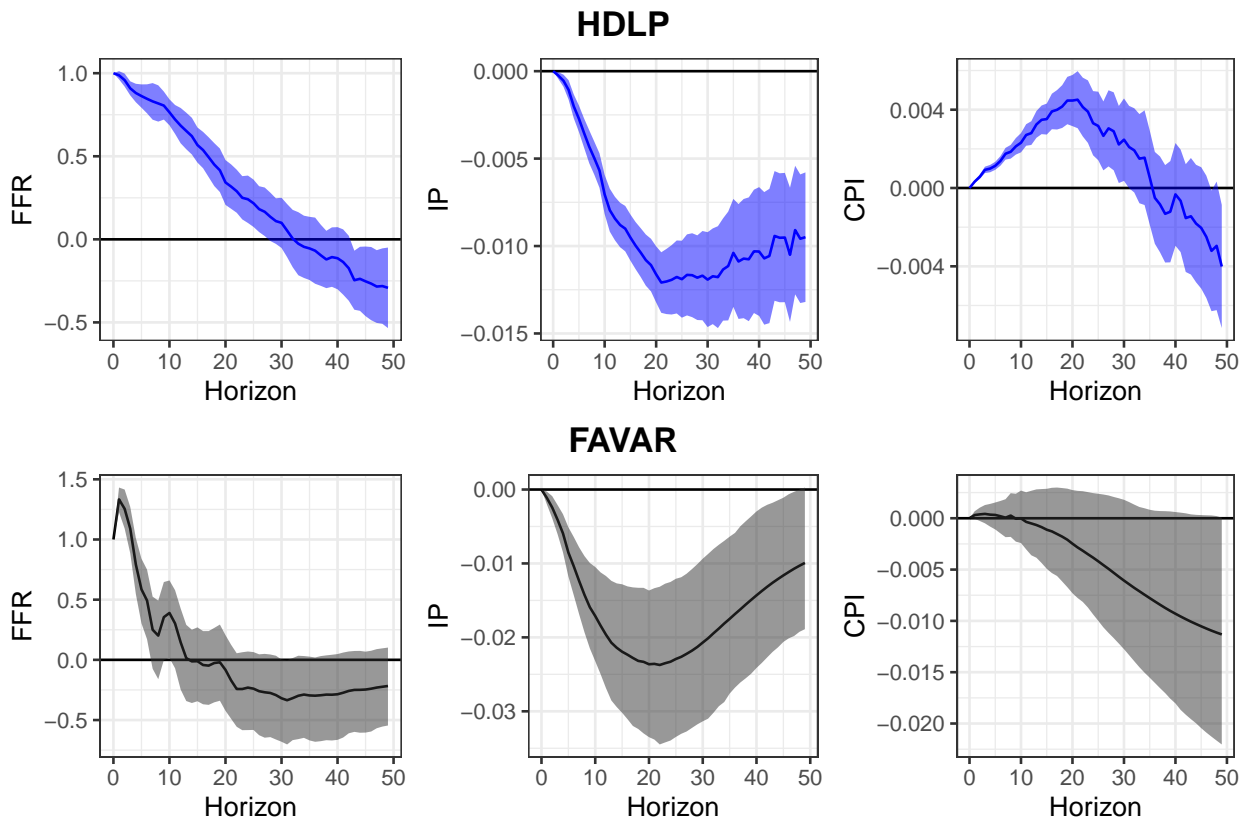


Figure 3: Estimated impulse responses with 95% confidence intervals of FFR, IP, and CPI to a monetary policy shock identified by the FFR for the HDLP and FAVAR.

are classified as slow, whereas those in the categories Interest & Exchange Rates, Money & Credit, Stock Market, and Housing as fast.<sup>7</sup> We apply the transformation codes of Bernanke et al. (2005) and McCracken and Ng (2016b) (for new variables) to remove stochastic trends. Using  $K = 13$  lags, the resulting HDLP consists of  $N = 1654$  regressors, while the time series length is  $T = 572$ .<sup>8</sup>

We compare the HDLP impulse responses obtained from the desparsified lasso to the ones obtained from a 3-factor FAVAR as used in Bernanke et al. (2005). Details about the FAVAR estimation are provided in Appendix C.3. Figure 3 shows the impulse responses of FFR, IP, and CPI to a shock in the FFR of a size such that the FFR has unit response at horizon 0. Since we use the first difference of IP and CPI in the model, we cumulate the impulse response which then corresponds to the response in the original (level) variables.<sup>9</sup> The comparable figure in Bernanke et al. (2005) is Figure 1.

The impulse responses from the FAVAR (bottom panel Figure 3) and HDLP (top panel) are generally similar. The impulse response of the FFR peaks at horizon 1 and then steadily declines to zero, which is in line with Figure 1 in Bernanke et al. (2005). For the HDLP, the response stays at a higher level for a longer period than for the FAVAR. The response of IP is also in line with

<sup>7</sup>One exception in the Category Prices is the series “OILPRICE<sub>x</sub>”, which we classify as fast.

<sup>8</sup>The exact number of variables in the model depends on which variable is taken as the response, and the effective number of observations depends on the horizon. These numbers are for the model where FFR is the response, at horizon 1.

<sup>9</sup>Cumulative impulse response functions for the HDLP are obtained by cumulating the dependent variable, i.e. taking  $\sum_{\ell=0}^h y_{t+\ell}$  on the LHS of eq. (2.1). For the FAVAR, we take the cumulative sum of the regular impulse responses from previous horizons. To ensure that these impulse responses are comparable, we scale the FAVAR impulse responses by the response of the FFR at horizon 0.

Bernanke et al. (2005), with the largest drop around horizon 20, before eventually returning to zero. Notably, the response obtained with the HDLP is considerably smaller than the one for the FAVAR. Finally for the response of CPI, we see a more pronounced price puzzle with the HDLP. The response is positive and significant for 30 months, peaking at horizon 20. The FAVAR impulse response is largely in line with Bernanke et al. (2005), with a small positive effect at early horizons, followed by a negative, though mainly insignificant, response after horizon 10.

## 4.2 Impulse Responses to a Shock in Government Spending

Ramey and Zubairy (2018) estimate impulse responses to a shock in US government spending identified based on military spending news. In this paper, we first augment the authors' main LP specification with more lags as a robustness check, before considering an extended state-dependent HDLP specification with interacting states related to unemployment and recession conditions. We use the quarterly data provided by the authors at [econweb.ucsd.edu/~vramey](http://econweb.ucsd.edu/~vramey) covering the period 1889Q1 to 2015Q4.

We estimate the state-dependent HDLP in Example 2.2 for real per capita GDP and government spending as  $y_t$ , while the shock variable  $x_t$  is the military spending news shock. We include taxes as controls in  $\mathbf{w}_{f,t}$ , while no variables are included in  $\mathbf{w}_{s,t}$ .<sup>10</sup> The state dummy variable  $I_t$  distinguishes between low and high unemployment states, with  $I_t = 1$  when unemployment in period  $t$  is larger than 6.5%. For full details on the construction of the shock variable and the treatment of the other variables, see section II.B of Ramey and Zubairy (2018). We use  $K = 40$  lags, such that the resulting HDLP consists of  $N = 464$  regressors, while the time series length is  $T = 161$ .<sup>11</sup>

Figure 4 shows the impulse responses to a shock in government spending. Note that the military spending news variable is scaled by GDP such that the impulse responses can be seen as a reaction to a shock of size 1% of GDP. The comparable figure in Ramey and Zubairy (2018) is Figure 5. The general shape and magnitude of these impulse responses are similar to the LP model with only 4 lags used in Ramey and Zubairy (2018). In our analysis, the peak of the responses in the high unemployment state occurs 2-3 quarters earlier, and experiences a sharper drop after horizon 15. We also find that the impulse response is not significant at horizon 0 in the linear and low-unemployment state.

Next to allowing the inclusion of more lags, the HDLP framework can easily be extended to allow for  $S$  states. The LP is then given by

$$y_{t+h} = \sum_{i=1}^S \alpha_i I_{i,t-1} + \sum_{i=1}^S I_{i,t-1} \left[ \phi_{i,h} x_t + \sum_{k=1}^K \delta'_{i,h,k} z_{t-k} \right] + u_{h,t}.$$

In addition to the unemployment state dummy  $I_t^{(U)}$ , we consider recession dummy  $I_t^{(R)}$ .<sup>12</sup> Letting them interact results in  $S = 4$  distinct state dummies.

Figure 5 displays the impulse response functions with four states. The impulse responses out of recessions resemble the state-dependent model of Figure 4, both in shape and magnitude, but we see a different pattern in the recession state. During recessions with low unemployment, there is

<sup>10</sup>While Ramey and Zubairy (2018) do not include taxes in their main analysis, they mention in footnote 11 that their results were robust to their inclusion. We prefer to include them as additional controls, following the VAR of Blanchard and Perotti (2002).

<sup>11</sup>As in Section 4.1, these correspond to the model estimated at horizon 1.

<sup>12</sup>As in Ramey and Zubairy (2018), we follow the NBER classification of recession periods.

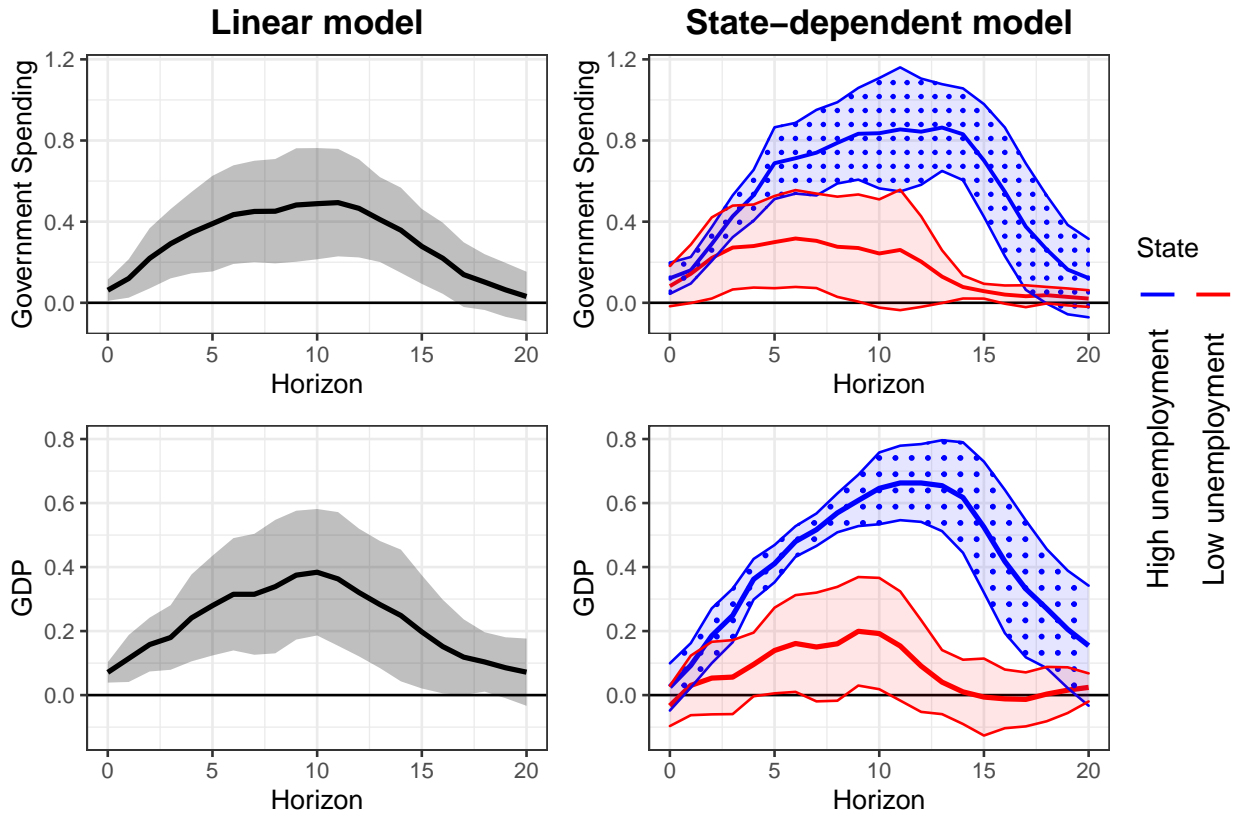


Figure 4: Estimated impulse responses with 95% confidence intervals of government spending and GDP to a government spending shock, in a model with 40 lags.

a negative impact response for both government spending and GDP, which becomes insignificant after a few periods. In the high unemployment state, in contrast, we see a large, positive, and persistent effect on both variables.

## 5 Conclusion

In this paper, we propose a modified version of the desparsified lasso to estimate local projections in high dimensions. The modification is simple, namely leaving the (small number of) dynamic impulse response parameter(s) of interest unpenalized in the initial lasso regression, yet provides considerable improvements in finite sample performance in terms of better coverage. The modified desparsified lasso estimator still comes with desirable asymptotic normality and uniformly valid asymptotic inference. Finally, we show how this method performs in a simulation using an empirically calibrated dynamic factor model and in canonical macroeconomic applications where we use the high-dimensional local projections framework to estimate structural impulse responses.

## Acknowledgements

We thank the co-editor and two referees for their thorough review which substantially improved the quality of the manuscript. The first and second author were financially supported by the Dutch Research Council (NWO) under grant number 452-17-010. Previous versions of this paper were presented at seminars at Aarhus University and ESSEC Business School, the NESG 2022

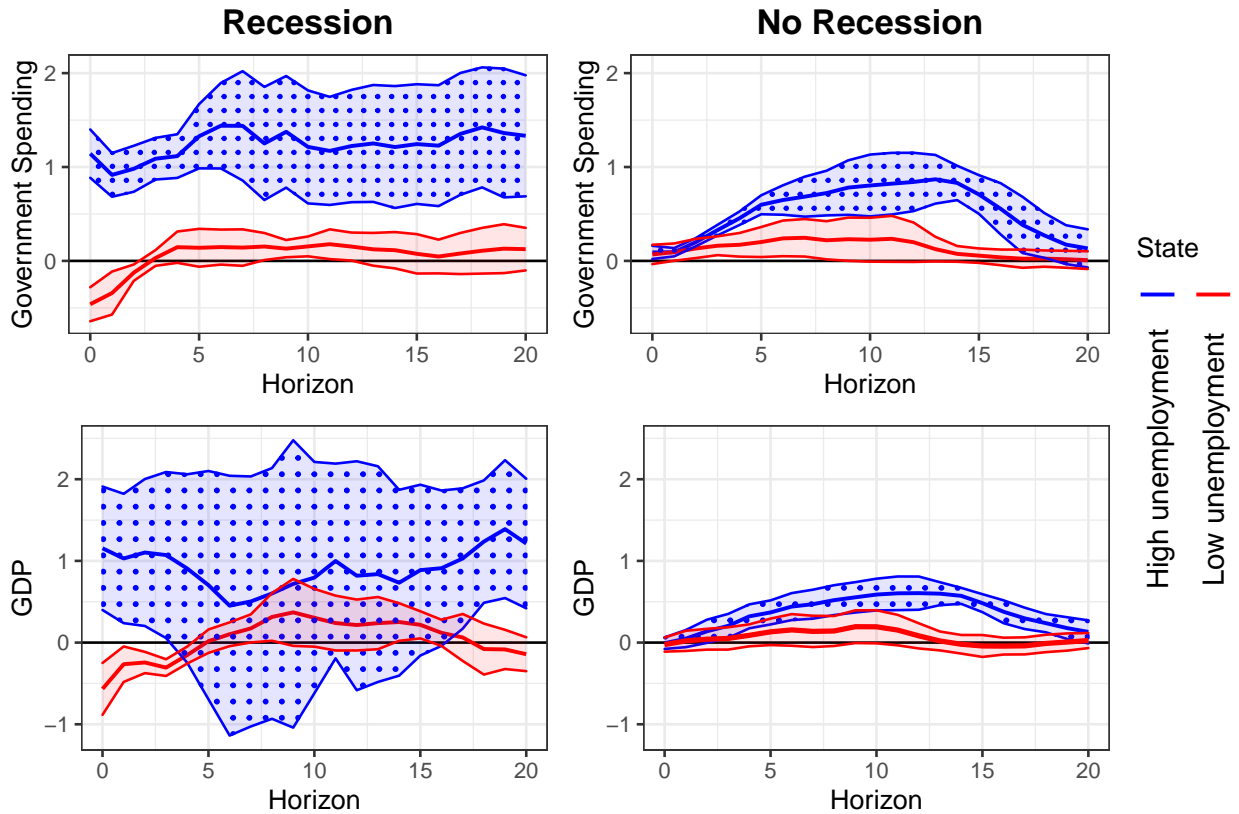


Figure 5: Estimated Impulse responses with 95% confidence intervals of government spending and GDP to a government spending shock.

conference and the 2022 Maastricht Workshop on Dimensionality Reduction and Inference in High-Dimensional Time Series. We gratefully acknowledge comments by participants at these seminars and conferences. We also thank Otilia Boldea and Lenard Lieb for helpful discussions. Remaining errors are our own.

## References

- Adamek, R., S. Smeekes, and I. Wilms (2022a). *desla: Desparsified Lasso Inference for Time Series*. R package version 0.2.0.
- Adamek, R., S. Smeekes, and I. Wilms (2022b). Lasso inference for high-dimensional time series. *Journal of Econometrics*, Forthcoming.
- Andrews, D. W. (1991). Heteroskedasticity and autocorrelation consistent covariance matrix estimation. *Econometrica* 59, 817–858.
- Angrist, J. D., Òscar Jordà, and G. M. Kuersteiner (2018). Semiparametric estimates of monetary policy effects: string theory revisited. *Journal of Business & Economic Statistics* 36, 371–387.
- Bañbura, M., D. Giannone, and L. Reichlin (2010). Large Bayesian vector auto regressions. *Journal of Applied Econometrics* 25, 71–92.
- Basu, S. and G. Michailidis (2015). Regularized estimation in sparse high-dimensional time series models. *Annals of Statistics* 43(4), 1535–1567.

- Belloni, A., V. Chernozhukov, and C. Hansen (2014). Inference on treatment effects after selection among high-dimensional controls. *Review of Economic Studies* 81, 608–650.
- Bernanke, B. S., J. Boivin, and P. Eliasch (2005). Measuring the effects of monetary policy: a factor-augmented vector autoregressive (FAVAR) approach. *Quarterly Journal of Economics* 120, 387–422.
- Bernanke, B. S. and I. Mihov (1998). Measuring monetary policy. *Quarterly Journal of Economics* 113, 869–902.
- Blanchard, O. and R. Perotti (2002). An empirical characterization of the dynamic effects of changes in government spending and taxes on output. *Quarterly Journal of Economics* 117, 1329–1368.
- Bühlmann, P. and S. van De Geer (2011). *Statistics for High-Dimensional Data: Methods, Theory and Applications*. Springer.
- Chan, J. C. (2020). Large Bayesian vector autoregressions. In P. Fuleky (Ed.), *Macroeconomic Forecasting in the Era of Big Data*, Volume 52 of *Advanced Studies in Theoretical and Applied Econometrics*, Chapter 4, pp. 95–125. Springer.
- Chen, K. and W. Wang (2022). *rrpack: Reduced-Rank Regression*. R package version 0.1-13.
- Christiano, L. J., M. Eichenbaum, and C. L. Evans (2005). Nominal rigidities and the dynamic effects of a shock to monetary policy. *Journal of Political Economy* 113, 1–45.
- Chudik, A. and M. H. Pesaran (2016). Theory and practice of GVAR modelling. *Journal of Economic Surveys* 30, 165–197.
- Davidson, J. (2002). *Stochastic Limit Theory* (2nd ed.). Oxford: Oxford University Press.
- Forni, M. and L. Gambetti (2014). Sufficient information in structural VARs. *Journal of Monetary Economics* 66, 124–136.
- Forni, M., D. Giannone, M. Lippi, and L. Reichlin (2009). Opening the black box: Structural factor models with large cross sections. *Econometric Theory* 25, 1319–1347.
- Gold, D., J. Lederer, and J. Tao (2020). Inference for high-dimensional instrumental variables regression. *Journal of Econometrics* 217(1), 79–111.
- Javanmard, A. and A. Montanari (2014). Confidence intervals and hypothesis testing for high-dimensional regression. *Journal of Machine Learning Research* 15, 2869–2909.
- Jordà, Ò. (2005). Estimation and inference of impulse responses by local projections. *American Economic Review* 95(1), 161–182.
- Karapanagioti, C. (2021). Model selection for local projections instrumental variable methods - empirical application to government spending multipliers. Master’s thesis, Tilburg University, Tilburg, The Netherlands.
- Kiefer, N. M. and T. J. Vogelsang (2005). A new asymptotic theory for heteroskedasticity-autocorrelation robust tests. *Econometric Theory* 21(6), 1130–1164.



- Kilian, L. and H. Lütkepohl (2017). *Structural Vector Autoregressive Analysis*. Themes in Modern Econometrics. Cambridge University Press.
- Kock, A. B. and L. Callot (2015). Oracle inequalities for high dimensional vector autoregressions. *Journal of Econometrics* 186, 325–344.
- Kock, A. B., M. Medeiros, and V. G (2020). Penalized regressions. In P. Fuleky (Ed.), *Macroeconomic Forecasting in the Era of Big Data*, Volume 52 of *Advanced Studies in Theoretical and Applied Econometrics*, Chapter 7, pp. 193–228. Springer.
- Koop, G., M. H. Pesaran, and S. M. Potter (1996). Impulse response analysis in nonlinear multivariate models. *Journal of Econometrics* 74, 119–147.
- Krampe, J., E. Paparoditis, and C. Trenkler (2022). Structural inference in sparse high-dimensional vector autoregressions. *Journal of Econometrics*, Forthcoming.
- Lazarus, E., D. J. Lewis, J. H. Stock, and M. W. Watson (2018). Har inference: Recommendations for practice. *Journal of Business & Economic Statistics* 36(4), 541–559.
- Leeb, H. and B. M. Pötscher (2005). Model selection and inference: Facts and fiction. *Econometric Theory* 21, 21–59.
- Li, D., M. Plagborg-Møller, and C. K. Wolf (2021). Local projections vs. vars: Lessons from thousands of dgps. arXiv e-print 2104.00655.
- Masini, R. P., M. C. Medeiros, and E. F. Mendes (2022). Regularized estimation of high-dimensional vector autoregressions with weakly dependent innovations. *Journal of Time Series Analysis* 43, 532–557.
- McCracken, M. W. and S. Ng (2016a). FRED-MD: a monthly database for macroeconomic research. *Journal of Business & Economic Statistics* 34, 574–589.
- McCracken, M. W. and S. Ng (2016b). FRED-MD: A monthly database for macroeconomic research. *Journal of Business & Economic Statistics* 34, 574–589.
- Montiel Olea, J. L. and M. Plagborg-Møller (2021). Local projection inference is simpler and more robust than you think. *Econometrica* 89, 1789–1823.
- Plagborg-Møller, M. and C. K. Wolf (2021). Local projections and VARs estimate the same impulse responses. *Econometrica* 89, 955–980.
- Ramey, V. A. (2016). Macroeconomic shocks and their propagation. In J. B. Taylor and H. Uhlig (Eds.), *Handbook of Macroeconomics*, Volume 2, pp. 71–162. Elsevier.
- Ramey, V. A. and S. Zubairy (2018). Government spending multipliers in good times and in bad: evidence from US historical data. *Journal of Political Economy* 126, 850–901.
- Romer, C. D. and D. H. Romer (2004). A new measure of monetary shocks: derivation and implications. *American Economic Review* 94(4), 1055–1084.
- Sims, C. A. (1980). Macroeconomics and reality. *Econometrica* 48, 1–48.

- Sims, C. A. and T. Zha (2006). Were there regime switches in U.S. monetary policy? *American Economic Review* 96(1), 54–81.
- Stock, J. and M. Watson (2016). Dynamic factor models, factor-augmented vector autoregressions, and structural vector autoregressions in macroeconomics. In J. B. Taylor and H. Uhlig (Eds.), *Handbook of Macroeconomics*, Volume 2, pp. 415–525. Elsevier.
- Stock, J. H. and M. W. Watson (2018). Identification and estimation of dynamic causal effects in macroeconomics using external instruments. *Economic Journal* 128, 917–948.
- Uematsu, Y. and T. Yamagata (2022a). Estimation of sparsity-induced weak factor models. *Journal of Business & Economic Statistics*, forthcoming.
- Uematsu, Y. and T. Yamagata (2022b). Inference in sparsity-induced weak factor models. *Journal of Business & Economic Statistics*, forthcoming.
- van de Geer, S., P. Bühlmann, Y. Ritov, and R. Dezeure (2014). On asymptotically optimal confidence regions and tests for high-dimensional models. *Annals of Statistics* 42, 1166–1202.
- van de Geer, S. A. (2016). *Estimation and testing under sparsity*. Springer.
- Wilms, I., D. S. Matteson, J. Bien, S. Basu, W. Nicholson, and E. Wegner (2021). *bigtime: Sparse Estimation of Large Time Series Models*. R package version 0.2.1.
- Yamada, H. (2017). The Frisch–Waugh–Lovell theorem for the lasso and the ridge regression. *Communications in Statistics-Theory and Methods* 46, 10897–10902.

## Appendix A: Assumptions

In the appendix, we use the following additional notation. For a matrix  $\mathbf{A}$ , we let  $\|\mathbf{A}\|_r = \max_{\|\mathbf{x}\|=1} \|\mathbf{A}\mathbf{x}\|_r$  for any  $r \in [0, \infty]$  and  $\|\mathbf{A}\|_{\max} = \max_{i,j} |a_{i,j}|$ .  $\Lambda_{\min}(\mathbf{A})$  denotes the minimum eigenvalue of  $\mathbf{A}$ . We frequently make use of arbitrary positive finite constants  $C$  (or its sub-indexed version  $C_i$ ) whose values may change from line to line throughout the paper, but they are always independent of the time and cross-sectional dimension. We say a sequence  $\eta_T$  is of size  $-x$  if  $\eta_T = O(T^{-x-\varepsilon})$  for some  $\varepsilon > 0$ .

**Assumption A.1.** *There exist some constants  $\bar{m} > m > 2$ , and  $d \geq \max\{1, (\bar{m}/m - 1)/(\bar{m} - 2)\}$  such that*

- (a)  $(\mathbf{x}'_t, u_t)'$  is a mean zero process with  $\mathbb{E}\mathbf{x}_t u_t = \mathbf{0}$  and  $\max_{1 \leq j \leq N} \mathbb{E}|x_{j,t}|^{2\bar{m}} \leq C$ ,  $\mathbb{E}|u_t|^{2\bar{m}} \leq C$ ,
- (b)  $\max_{1 \leq j \leq S} \mathbb{E}|v_{j,t}|^{2\bar{m}} \leq C$ ,
- (c) Let  $\{\boldsymbol{\epsilon}_{T,t}\}$  denote a  $k(T)$ -dimensional triangular array that is  $\alpha$ -mixing of size  $-d/(1/m - 1/\bar{m})$  with  $\sigma$ -field  $\mathcal{F}_t^\epsilon := \sigma\{\boldsymbol{\epsilon}_{T,t}, \boldsymbol{\epsilon}_{T,t-1}, \dots\}$  such that  $(\mathbf{x}'_t, u_t)'$  is  $\mathcal{F}_t^\epsilon$ -measurable. The processes  $u_t$  and  $x_{j,t}$  are  $L_{2m}$ -near-epoch-dependent (NED) of size  $-d$  on  $\boldsymbol{\epsilon}_{T,t}$  with positive bounded constants, uniformly over  $j = 1, \dots, N$ .

**Assumption A.2.** For some  $0 \leq r < 1$  and sparsity level  $s_r$ , define the  $N$ -dimensional sparse compact parameter space  $\mathbf{B}_N(r, s_r) := \{\boldsymbol{\beta} \in \mathbb{R}^N : \|\boldsymbol{\beta}\|_r \leq s_r, \|\boldsymbol{\beta}\|_{\max} \leq C, \exists C < \infty\}$ . Then (a)  $\boldsymbol{\beta} \in \mathbf{B}_N(r, s_r)$  and (b)  $\boldsymbol{\gamma}_j \in \mathbf{B}_{N-1}(r, s_{r,j})$  for all  $j \in \mathcal{H}$ , where  $\boldsymbol{\gamma}_j = \arg \min_{\boldsymbol{\gamma}_j^* \in \mathbb{R}^{N-1}} \mathbb{E} \left\| \mathbf{x}_j - \mathbf{X}_{-j} \boldsymbol{\gamma}_j^* \right\|_2^2 / T$ .

**Assumption A.3.** Let  $\Lambda_{\min}(\boldsymbol{\Sigma})$  denote the smallest eigenvalue of  $\boldsymbol{\Sigma} = \mathbb{E} \mathbf{X}' \mathbf{X} / T$ , and  $\Lambda_{\min}(\boldsymbol{\Omega}_{N,T})$  the smallest eigenvalue of  $\boldsymbol{\Omega}_T := \mathbb{E} \left[ \frac{1}{T} \left( \sum_{t=1}^T \mathbf{q}_t \right) \left( \sum_{t=1}^T \mathbf{q}_t' \right) \right]$ . Assume that  $1/C \leq \Lambda_{\min}(\boldsymbol{\Sigma}) \leq C$ , and  $1/C \leq \Lambda_{\min}(\boldsymbol{\Omega}_{N,T}) \leq C$ .

**Assumption A.4.**  $H \leq C$ , where  $H$  is the cardinality of  $\mathcal{H}$ .

**Assumption A.5.** Let  $\lambda_{\min} := \min\{\lambda, \min_j \lambda_j\}$ ,  $\lambda_{\max} := \max\{\lambda, \max_j \lambda_j\}$ , and  $s_{r,\max} := \max\{s_r, \max_j s_{r,j}\}$ . Then  $Q_T T^{-\frac{1}{2/d+2m/(m-2)}} \rightarrow 0$  for  $Q_T \rightarrow \infty$ ,  $\lambda \sim \lambda_{\max} \sim \lambda_{\min}$ , and

$$\begin{aligned} 0 < r < 1: \quad & (\ln \ln T)^{-1} s_{r,\max}^{1/r} \left[ \frac{N^{\left(\frac{2}{d} + \frac{2}{m-1}\right)}}{\sqrt{T}} \right]^{\frac{1}{r\left(\frac{1}{d} + \frac{m}{m-1}\right)}} \leq \lambda \\ & \leq \ln \ln T \left[ Q_T^2 \sqrt{T} s_{r,\max} \right]^{-1/(2-r)}, \\ r = 0: \quad & (\ln \ln T)^{-1} \frac{N^{1/m}}{\sqrt{T}} \leq \lambda \leq \ln \ln T \left[ Q_T^2 \sqrt{T} s_{0,\max} \right]^{-1/2}. \end{aligned}$$

These bounds are feasible when  $Q_T^r s_{r,\max} N^{(2-r)\left(\frac{d+m-1}{dm+m-1}\right)} T^{\frac{1}{4}\left(r - \frac{d(m-1)(2-r)}{dm+m-1}\right)} \rightarrow 0$ , and additionally when  $Q_T^2 s_{0,\max} \frac{N^{2/m}}{\sqrt{T}} \rightarrow 0$  if  $r = 0$ .

## Appendix B: Proofs

**Lemma B.1.** Take a vector  $\{\mathbf{z} \in \mathbb{R}^N : \|\mathbf{z}_{\mathcal{H}^c}\|_1 \leq 3 \|\mathbf{z}_{\mathcal{H}}\|_1\}$ , an index set  $\mathcal{H}$  with cardinality  $|\mathcal{H}|$  and define the subscript operator  $\mathbf{z}_{\mathcal{H}} := \{\mathbf{z}^* \in \mathbb{R}^N : z_j^* = z_j \mathbf{1}_{\{j \in \mathcal{H}\}}\}$ . Under Assumption A.3, on the set  $\mathcal{CC}_T(\mathcal{H}) := \left\{ \left\| \hat{\boldsymbol{\Sigma}} - \boldsymbol{\Sigma} \right\|_{\max} \leq C/|\mathcal{H}| \right\}$ ,

$$\|\mathbf{z}_{\mathcal{H}}\|_1 \leq \sqrt{\frac{2|\mathcal{H}| \mathbf{z}' \hat{\boldsymbol{\Sigma}} \mathbf{z}}{\Lambda_{\min}}}$$

**Proof:** By Lemma 6.17 and Corollary 6.8 in Bühlmann and van De Geer (2011), this result holds for the “ $\boldsymbol{\Sigma}$ -compatibility condition”. By Lemma 6.23 in Bühlmann and van De Geer (2011), this compatibility condition holds under Assumption A.3, and the result follows from the fact that  $\Lambda_{\min}$  bounds the compatibility constant from below.  $\square$

**Lemma B.2.** Let  $P$  be an index set with cardinality  $|P|$  such that  $\mathcal{H} \subseteq P$ . Define the set  $\mathcal{E}_T(z) = \{\max_{j \leq N, s \leq T} \left\| \sum_{t=1}^s u_t \mathbf{x}_{j,t} \right\| \leq z\}$ . Under Assumption A.3, on  $\mathcal{E}_T(T^{\frac{\lambda}{4}}) \cap \mathcal{CC}_T(P)$ :

$$T^{-1} \left\| \mathbf{X}(\hat{\boldsymbol{\beta}}^{(L)} - \boldsymbol{\beta}) \right\|_2^2 + \lambda/4 \left\| \hat{\boldsymbol{\beta}}^{(L)} - \boldsymbol{\beta} \right\|_1 \leq C_1 \lambda^2 |P| + C_2 \lambda \|\boldsymbol{\beta}_{P^c}\|.$$

**Proof:** The proof closely follows the proof of Lemma A.6 in Adamek et al. (2022b), based on Theorem 2.2 of van de Geer (2016), with small modifications to handle the penalty matrix  $\mathbf{W}$ . From the Lasso optimization problem in eq. (2.5), we have the Karush-Kuhn-Tucker (KKT) conditions

$T^{-1}\mathbf{X}'(\mathbf{y} - \mathbf{X}\hat{\boldsymbol{\beta}}^{(L)}) = \mathbf{W}\hat{\boldsymbol{\kappa}}^*\lambda$ , where  $\hat{\boldsymbol{\kappa}}^* = (\mathbf{0}_{1 \times H}, \hat{\boldsymbol{\kappa}})'$ , and  $\hat{\boldsymbol{\kappa}}$  is the subdifferential of  $\|\hat{\boldsymbol{\beta}}_{-\mathcal{H}}^{(L)}\|_1$ . This then leads to the inequality

$$\begin{aligned} T^{-1}(\boldsymbol{\beta} - \hat{\boldsymbol{\beta}}^{(L)})'\mathbf{X}'(\mathbf{y} - \mathbf{X}\hat{\boldsymbol{\beta}}^{(L)}) &= (\boldsymbol{\beta} - \hat{\boldsymbol{\beta}}^{(L)})'\mathbf{W}\hat{\boldsymbol{\kappa}}^*\lambda = \boldsymbol{\beta}'\mathbf{W}\hat{\boldsymbol{\kappa}}^*\lambda - \hat{\boldsymbol{\beta}}^{(L)'}\mathbf{W}\hat{\boldsymbol{\kappa}}^*\lambda \\ &\leq \lambda\|\mathbf{W}'\boldsymbol{\beta}\|_1 - \lambda\|\mathbf{W}'\hat{\boldsymbol{\beta}}^{(L)}\|_1. \end{aligned}$$

To deal with the matrix  $\mathbf{W}$  in these expressions, we use the bound  $\|\mathbf{W}'(\hat{\boldsymbol{\beta}}_P^{(L)} - \boldsymbol{\beta}_P)\|_1 \leq \|\hat{\boldsymbol{\beta}}_P^{(L)} - \boldsymbol{\beta}_P\|_1$  and the property that  $\|\mathbf{W}'\mathbf{z}_{P^c}\|_1 = \|\mathbf{z}_{P^c}\|_1$  for  $\mathbf{z} \in \mathbb{R}^N$ , since  $\mathcal{H} \subseteq P$ , and those elements set to zero by  $\mathbf{W}$  are already zero due to subscript  $P^c$  operator. Using these additional arguments, we can show that

$$T^{-1}\|\mathbf{X}(\hat{\boldsymbol{\beta}}^{(L)} - \boldsymbol{\beta})\|_2^2 \leq \frac{5\lambda}{4}\|\hat{\boldsymbol{\beta}}_P^{(L)} - \boldsymbol{\beta}_P\|_1 - \frac{3\lambda}{4}\|\hat{\boldsymbol{\beta}}_{P^c}^{(L)} - \boldsymbol{\beta}_{P^c}\|_1 + 2\lambda\|\boldsymbol{\beta}_{P^c}\|_1,$$

and the remainder of the proof is analogous to the proof of Lemma A.6 in Adamek et al. (2022b), using Lemma B.1 instead of Lemma A.5 in Adamek et al. (2022b).  $\square$

**Lemma B.3.** *Under Assumptions A.1 to A.4, for any*

$$\begin{aligned} 0 < r < 1: \quad \lambda &\geq C \ln(\ln(T))^{\frac{d+m-1}{r(dm+m-1)}} \left[ s_r \left( \frac{N^{\left(\frac{2}{d} + \frac{2}{m-1}\right)}}{\sqrt{T}} \right)^{\frac{1}{\left(\frac{1}{d} + \frac{m}{m-1}\right)}} \right]^{\frac{1}{r}} \\ r = 0: \quad s_0 &\leq C \ln(\ln(T))^{-\frac{d+m-1}{dm+m-1}} \left[ \frac{\sqrt{T}}{N^{\left(\frac{2}{d} + \frac{2}{m-1}\right)}} \right]^{\frac{1}{\left(\frac{1}{d} + \frac{m}{m-1}\right)}}, \\ \lambda &\geq C \ln(\ln(T))^{1/m} \frac{N^{1/m}}{\sqrt{T}} \end{aligned} \tag{B.9}$$

and when  $N, T$  are sufficiently large, the following holds with probability at least  $1 - v_{N,T}^{\mathcal{C}\mathcal{C}} - v_{N,T}^{\mathcal{E}}$ :

$$(i) \quad \frac{1}{T}\|\mathbf{X}(\hat{\boldsymbol{\beta}}^{(L)} - \boldsymbol{\beta})\|_2^2 \leq C\lambda^{2-r}s_r, \quad (ii) \quad \|\hat{\boldsymbol{\beta}}^{(L)} - \boldsymbol{\beta}\|_1 \leq C\lambda^{1-r}s_r,$$

where  $v_{N,T}^{\mathcal{C}\mathcal{C}}$  and  $v_{N,T}^{\mathcal{E}}$  are sequences that converge to 0 for large  $T, N$  (defined formally in the proof).

**Proof:** Let  $P_\lambda := \{j : |\beta_j| > \lambda\}$ , and  $P_{\mathcal{H},\lambda} := \mathcal{H} \cup P_\lambda$ , such that by construction,  $\mathcal{H} \subseteq P_{\mathcal{H},\lambda}$ . It then follows that by Assumption A.3 and Lemma B.2, we have on the set  $\mathcal{E}_T(T^{\frac{\lambda}{4}}) \cap \mathcal{C}\mathcal{C}_T(P_{\mathcal{H},\lambda})$

$$\|\mathbf{X}(\hat{\boldsymbol{\beta}}^{(L)} - \boldsymbol{\beta})\|_2^2 / T + \frac{\lambda}{4}\|\hat{\boldsymbol{\beta}}^{(L)} - \boldsymbol{\beta}\|_1 \leq C_1\lambda^2|P_{\mathcal{H},\lambda}| + C_2\lambda\|\boldsymbol{\beta}_{P_{\mathcal{H},\lambda}^c}\|_1.$$

It follows directly from Assumption A.2 that

$$|P_{\mathcal{H},\lambda}| \leq H + \sum_{j=1}^N \mathbb{1}_{\{|\beta_j| > \lambda\}} \left( \frac{|\beta_j|}{\lambda} \right)^r \leq H + \lambda^{-r} \sum_{j=1}^N |\beta_j|^r = H + \lambda^{-r}s_r.$$

Note that since  $H \leq C$  by Assumption A.4 and both  $\lambda^{-r}$  and  $s_r$  asymptotically grow as  $N, T \rightarrow \infty$ , for sufficiently large  $N$  and  $T$ ,  $H + \lambda^{-r}s_r \leq C\lambda^{-r}s_r$ . Following the proof of Lemma A.7 in Adamek et al. (2022b), we can also show that  $\|\boldsymbol{\beta}_{P_{\mathcal{H},\lambda}^c}\|_1 \leq \lambda^{1-r}s_r$ , and obtain the error bound

$$T^{-1}\|\mathbf{X}(\hat{\boldsymbol{\beta}}^{(L)} - \boldsymbol{\beta})\|_2^2 + \lambda\|\hat{\boldsymbol{\beta}}^{(L)} - \boldsymbol{\beta}\|_1 \leq C_1\lambda^{2-r}s_r + C_2\lambda^{2-r}s_r = C\lambda^{2-r}s_r.$$

For the set  $\mathcal{CC}_T(P_{\mathcal{H},\lambda})$ , under Assumptions A.1 to A.3, we can apply Lemma A.3 in Adamek et al. (2022b) with  $\eta_T = 1/\ln(\ln(T)) \frac{d+m-1}{d+m-1}$  to show that  $\mathbb{P}(\mathcal{CC}_T(P_\lambda)) \geq 1 - 3 [1/\ln(\ln(T))] \frac{d+m-1}{d+m-1} := 1 - v_{N,T}^{\mathcal{CC}} \rightarrow 1$  as  $N, T \rightarrow \infty$ . Note that the condition  $\eta_T \leq \frac{N^2}{e}$  is satisfied for sufficiently large  $N, T$ , and we also use this in the proof of Lemma A.3 in Adamek et al. (2022b) to plug in  $|P_{\mathcal{H},\lambda}| \leq H + \lambda^{-r} s_r \leq C\lambda^{-r} s_r$ .

Regarding the set  $\mathcal{E}_T(T\frac{\lambda}{4})$ , by Assumption A.1 and Lemma A.4 in Adamek et al. (2022b),  $\mathbb{P}(\mathcal{E}_T(T\lambda/4)) \geq 1 - CN(\sqrt{T}\lambda)^{-m} := 1 - v_{N,T}^{\mathcal{E}}$ . By the union bound,

$$\mathbb{P}(\mathcal{E}_T(T\lambda/4) \cap \mathcal{CC}_T(P_{\mathcal{H},\lambda})) \geq 1 - v_{N,T}^{\mathcal{E}} - v_{N,T}^{\mathcal{CC}},$$

and therefore the error bound holds with this probability as well. With the error bound, items (i) and (ii) follow straightforwardly.  $\square$

**Proof of Theorem 2.1:** This result follows from Corollary 2 of Adamek et al. (2022b), with some small differences summarized here. First, in Adamek et al. (2022b), the tested hypotheses involve the full vector of parameters  $\beta$ , whereas our result only holds for  $\beta_{\mathcal{H}}$ . However, the matrix  $\mathbf{R}_N$  in Adamek et al. (2022b) is restricted to have only  $H$  nonzero columns such that  $\{j : \sum_{p=1}^P |r_{p,j}| > 0\} = \mathcal{H}$ . The setup here is therefore equivalent to taking  $\mathbf{R}_N = \begin{pmatrix} \mathbf{I} & \mathbf{0} \\ \mathbf{0} & \mathbf{0} \end{pmatrix}_{H \times H, H \times (N-H)}$ , and the elements we omit here are equal to zero.

Second, parts of the proof which require bounds on  $\|\hat{\beta}^{(L)} - \beta\|_1$  or  $\|\hat{\mathbf{u}}^{(L)} - \mathbf{u}\|_2$  need to be addressed by the new lasso error bound in Lemma B.3, rather than by Corollary 1 in Adamek et al. (2022b). Specifically, in Lemma B.8 of Adamek et al. (2022b) we need the bound  $\|\hat{\beta}^{(L)} - \beta\|_1 \leq C\lambda^{1-r} s_r$ , and in Lemma B.13 of Adamek et al. (2022b) we need  $\|\hat{\mathbf{u}} - \mathbf{u}\|_2 = \|\mathbf{X}(\hat{\beta}^{(L)} - \beta)\|_2 \leq C\sqrt{T}\lambda^{2-r} s_r$ . Note that since the new lasso error bound is the same as for the regular lasso, no changes to these proofs are necessary.  $\square$

## Appendix C: Supplementary

### C.1 Simulations: Implementation Details and Extra Figures

This section contains the implementation details and additional figures for our simulation experiments, Section 3.

#### C.1.1 Sparse Structural VAR Model

Consider the DGP

$$\begin{pmatrix} y_t \\ \mathbf{w}_{s,t} \end{pmatrix} = \mathbf{z}_t = \sum_{k=1}^4 \mathbf{A}_k \mathbf{z}_{t-k} + \boldsymbol{\epsilon}_t, \quad \boldsymbol{\epsilon}_t \stackrel{iid}{\sim} N(\mathbf{0}, \mathbf{I}), \quad (\text{C.1})$$

where the autoregressive parameter matrices  $\mathbf{A}_k$  are tapered Toeplitz matrices for which we consider two different settings. In the first setting, we take  $(\mathbf{A}_k)_{i,j} = \rho_k^{|i-j|+1}$  if  $|i-j| < P/2$  and 0 otherwise, and  $(\rho_1, \rho_2, \rho_3, \rho_4) = (0.2, 0.15, 0.1, 0.05)$ . In the second setting, we simply switch the signs of all entries in the second and fourth autoregressive parameter matrices. We consider different values for the number of variables  $P = \{20, 40, 100\}$  and time series length  $T = \{100, 200, 500\}$ .<sup>13</sup> Equation (C.1) can be seen as a simple structural VAR with structural shocks  $\boldsymbol{\epsilon}_t$ . The true impulse responses are obtained by inverting the lag polynomial, rewriting it as  $\mathbf{x}_t = \sum_{k=0}^{\infty} \mathbf{B}_k \boldsymbol{\epsilon}_{t-k} = \mathbf{B}(L)\boldsymbol{\epsilon}_t$ , where  $\mathbf{B}(L) = \mathbf{A}(L)^{-1} = \left(\mathbf{I} - \sum_{k=1}^4 \mathbf{A}_k L^k\right)^{-1}$  and  $\mathbf{B}_0 = \mathbf{I}$ . We analyse the response of  $y_t$  to the first shock  $\epsilon_{1,t}$  using local projections

$$y_{t+h} = \phi_h y_t + \boldsymbol{\eta}'_h \mathbf{w}_{s,t} + \sum_{k=1}^K \boldsymbol{\delta}'_{h,k} \mathbf{z}_{t-k} + u_{h,t}, \quad h = 1, \dots, h_{\max},$$

and obtain estimates of the impulse responses  $\hat{\phi}_1, \dots, \hat{\phi}_{h_{\max}}$  with  $h_{\max} = 10$  and  $K = 4$ .<sup>14</sup>

Figure C.1 presents the coverage rates all values of  $P$  and  $T$  of the proposed desparsified lasso (blue), which leaves the impulse response parameters of interest unpenalized, in comparison to the standard desparsified lasso (red). Figure C.2 displays the corresponding interval widths.

#### C.1.2 Empirically Calibrated Dynamic Factor Model

We consider an empirically calibrated dynamic factor model in the spirit of Lazarus et al. (2018) and Li et al. (2021), which we estimate based on 122 monthly variables  $\mathbf{x}_t$  from the FRED-MD database (McCracken and Ng, 2016a).<sup>15</sup> The DFM is given by

$$\mathbf{x}_t = \boldsymbol{\Lambda} \mathbf{f}_t + \mathbf{v}_t, \quad (\text{C.2})$$

$$\mathbf{f}_t = \boldsymbol{\Phi} \mathbf{f}_{t-1} + \mathbf{H} \boldsymbol{\epsilon}_t, \quad (\text{C.3})$$

$$v_{i,t} = \Delta_i(L) v_{i,t-1} + \Xi_i \xi_{i,t}, \quad (\text{C.4})$$

where eq. (C.2) describes the 6-factor model for  $\mathbf{X}_t$ , eq. (C.3) describes the VAR(1) model for the factors, and eq. (C.4) gives the individual AR(2) models for the idiosyncratic errors from the factor

<sup>13</sup>The number of regressors in the model is  $N = 5P$ , due to the included lags.

<sup>14</sup>At horizon 0 the response is  $(\mathbf{B}_0)_{1,1} = 1$  by our identification scheme, and thus does not need to be estimated.

<sup>15</sup>The variables are detailed in section C.2.

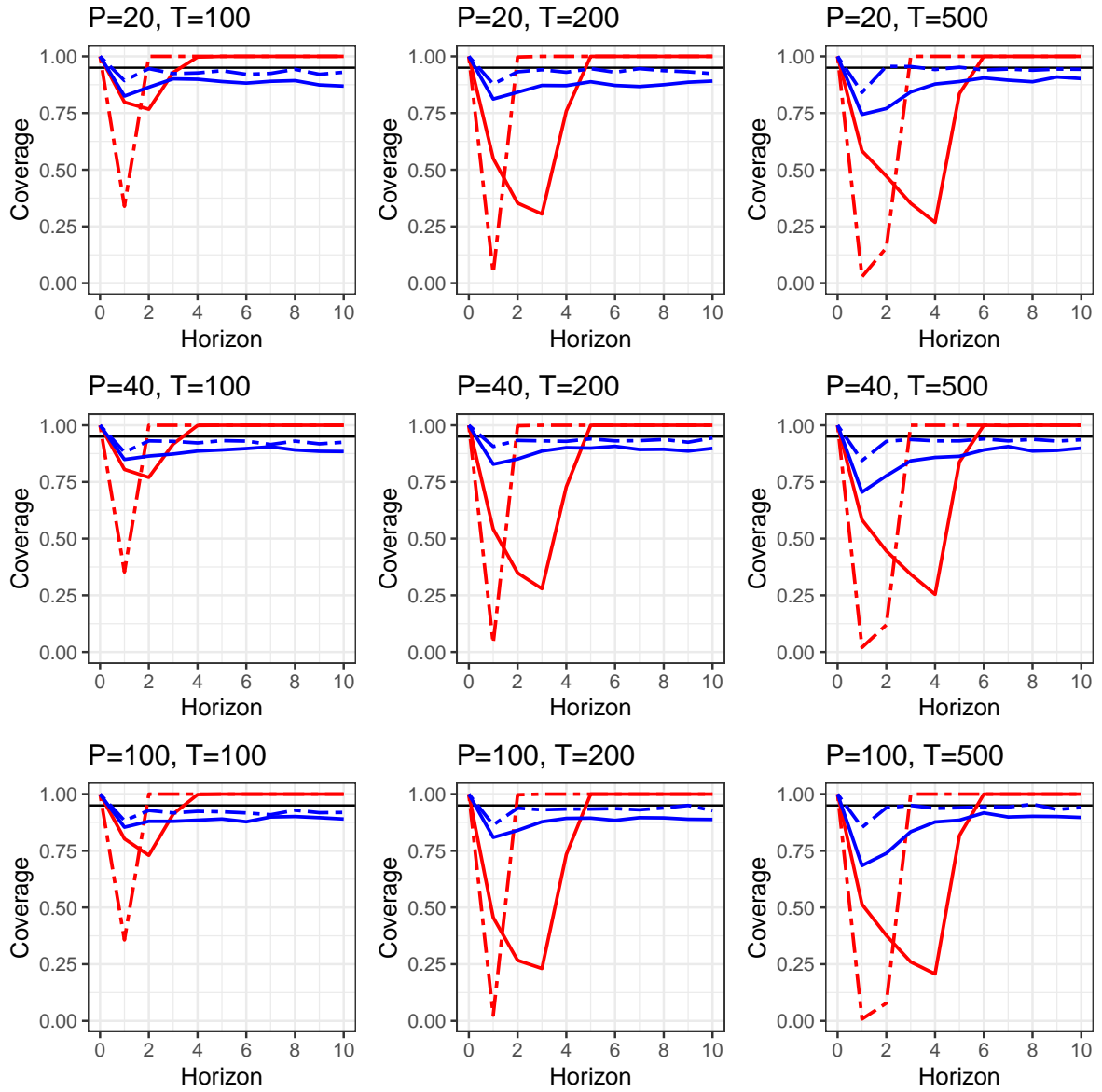


Figure C.1: Coverage of the standard desparsified lasso (red) and the proposed desparsified lasso with  $\phi_h$  unpenalized (blue). Dashed lines indicate results for the sign-switching DGP.

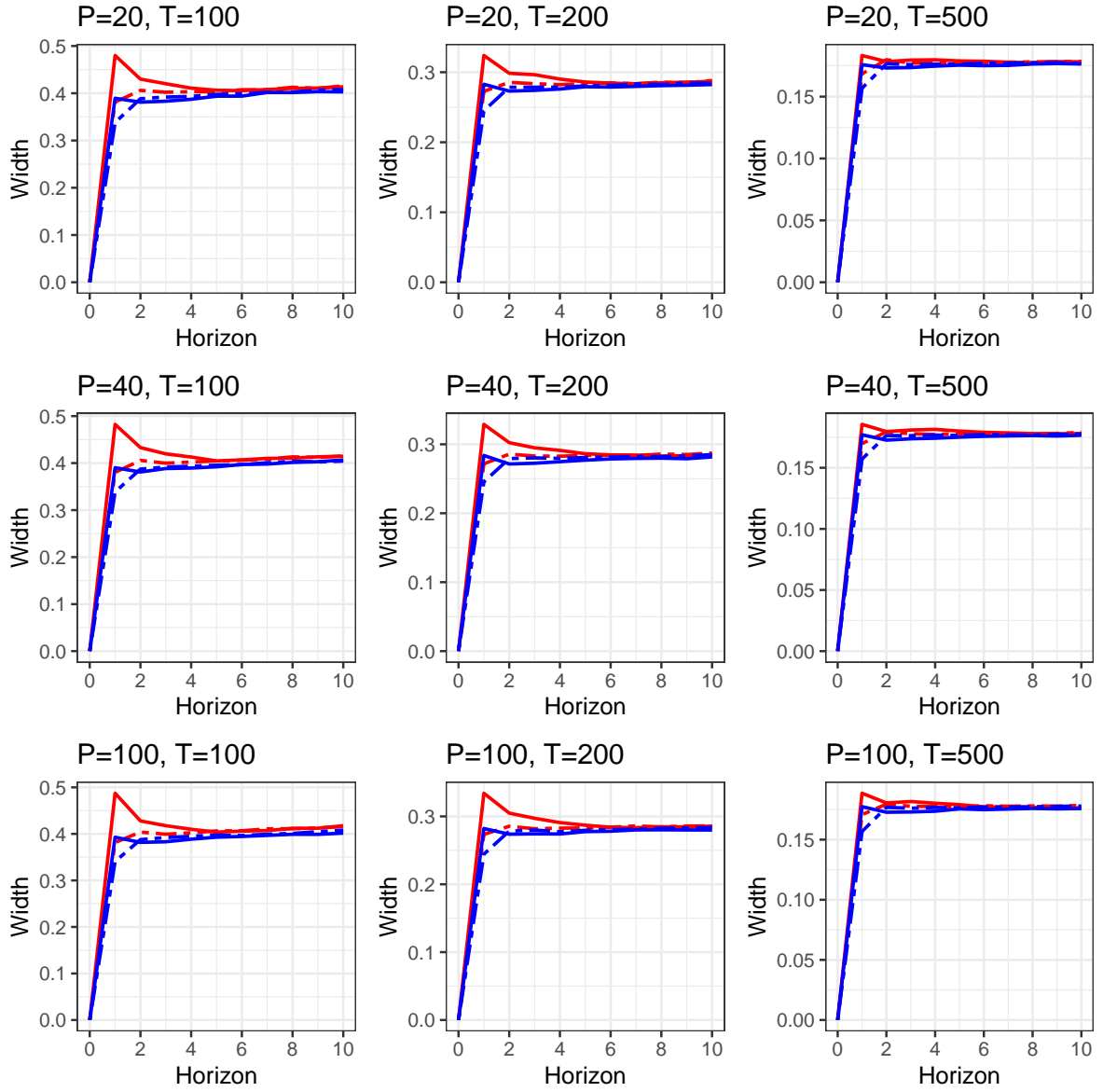


Figure C.2: Interval widths of the standard desparsified lasso (red) and the proposed desparsified lasso with  $\phi_h$  unpenalized (blue). Dashed lines indicate results for the sign-switching DGP.

model. Note that we can re-write eq. (C.4) as  $\mathbf{v}_t = \mathbf{\Delta}(L)\mathbf{v}_{t-1} + \mathbf{\Xi}\xi_t$ , with  $\mathbf{\Delta}$  and  $\mathbf{\Xi}$  diagonal.

We consider two different versions of this DFM: A “dense” DFM where we set  $\mathbf{\Lambda} = \hat{\mathbf{\Lambda}}_{PC}$  and  $\mathbf{\Phi} = \hat{\mathbf{\Phi}}_{OLS}$ , with  $\hat{\mathbf{\Lambda}}_{PC}$  obtained using principal components and  $\hat{\mathbf{\Phi}}_{OLS}$  obtained by fitting a VAR(1) on the estimated factors by OLS; and a “sparse” DFM, where  $\mathbf{\Lambda} = \hat{\mathbf{\Lambda}}_{WF}$  and  $\mathbf{\Phi} = \hat{\mathbf{\Phi}}_L$ , with  $\hat{\mathbf{\Lambda}}_{WF}$  obtained using the WF-SOFAR estimator of Uematsu and Yamagata (2022a) and  $\hat{\mathbf{\Phi}}_L$  by fitting the VAR(1) with the lasso.<sup>16</sup> To see the differences in sparsity between the dense and sparse specifications, see Figure C.3; the top row of plots compares the number of nonzero entries and  $L_1$ -norms for each column of  $\mathbf{\Lambda}$ , the bottom shows heatmaps of  $\mathbf{\Phi}$ .

After fitting the models as described above, we use the residuals  $\hat{\mathbf{e}}_t = \hat{\mathbf{f}}_t - \hat{\mathbf{\Phi}}\hat{\mathbf{f}}_{t-1}$  and  $\hat{\boldsymbol{\zeta}}_t = \hat{\mathbf{v}}_t - \hat{\mathbf{\Delta}}(L)\hat{\mathbf{v}}_{t-1}$  to compute the sample covariances  $\hat{\boldsymbol{\Sigma}}_e = \frac{1}{T-1} \sum_{t=2}^T \hat{\mathbf{e}}_t \hat{\mathbf{e}}_t'$  and  $\hat{\boldsymbol{\Sigma}}_\zeta$  with  $\hat{\sigma}_{\zeta,i}^2 = \frac{1}{T-2} \sum_{t=3}^T \hat{\zeta}_{i,t}^2$  on the diagonal and 0 otherwise. Following Li et al. (2021), we then choose  $\mathbf{H}$  as a function of  $\hat{\mathbf{\Lambda}}$

<sup>16</sup>We use the WF-SOFAR estimator with BIC criterion as implemented in the R package `rrpack` (Chen and Wang, 2022), see Section D of the supplementary material to Uematsu and Yamagata (2022a) for further details. For the lasso VAR, we use the estimator with BIC criterion implemented in the R package `bigtime` (Wilms et al., 2021).



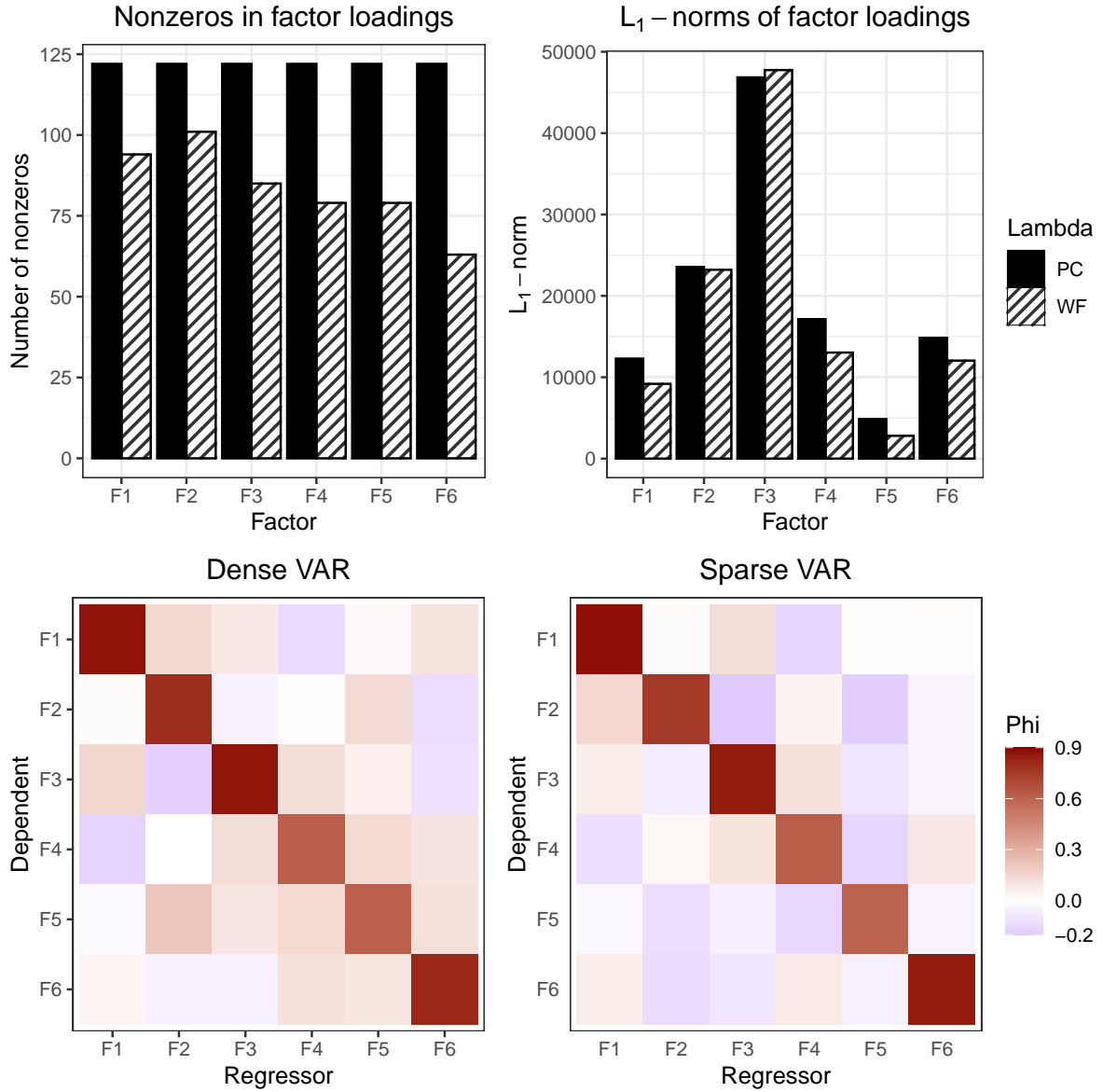


Figure C.3: Differences in sparsity between the dense and sparse DFM models.

and  $\hat{\Sigma}_e$  which maximises the contemporaneous effect of  $\epsilon_{1,t}$  on the Federal Funds Rate (FFR), the monetary policy instrument in this simulation; for details, see Appendix A.2 of Li et al. (2021). We take  $\Xi = \hat{\Sigma}_\zeta^{-1/2}$ . We use a recursive identification scheme similar to that of Li et al. (2021), where we order Industrial Production (IP) first, FFR last, and estimate the impulse response of IP to FFR. As noted in Section 3.2 of Li et al. (2021), the shock identified in this way is not necessarily structural, i.e., it does not necessarily correspond to any specific shock in  $\epsilon_t$  or  $\xi_t$ . To compute the true impulse response implied by the calibrated model, we use the state-space representation described in Appendix A.4 of Li et al. (2021). The data in the simulations are generated as in eqs. (C.2) to (C.4) with  $\epsilon_t \stackrel{iid}{\sim} N(\mathbf{0}, \mathbf{I})$  and  $\xi_t \stackrel{iid}{\sim} N(\mathbf{0}, \mathbf{I})$ , at sample lengths  $T = \{200, 400, 600\}$  with 1000 replications.

### C.1.3 Sensitivity of HDLP to the Long-run Covariance Estimator

We investigate the sensitivity of the proposed HDLP estimator to the choice of long-run covariance estimator. In addition to our default choice of Newey-West, we consider two alternative estimators

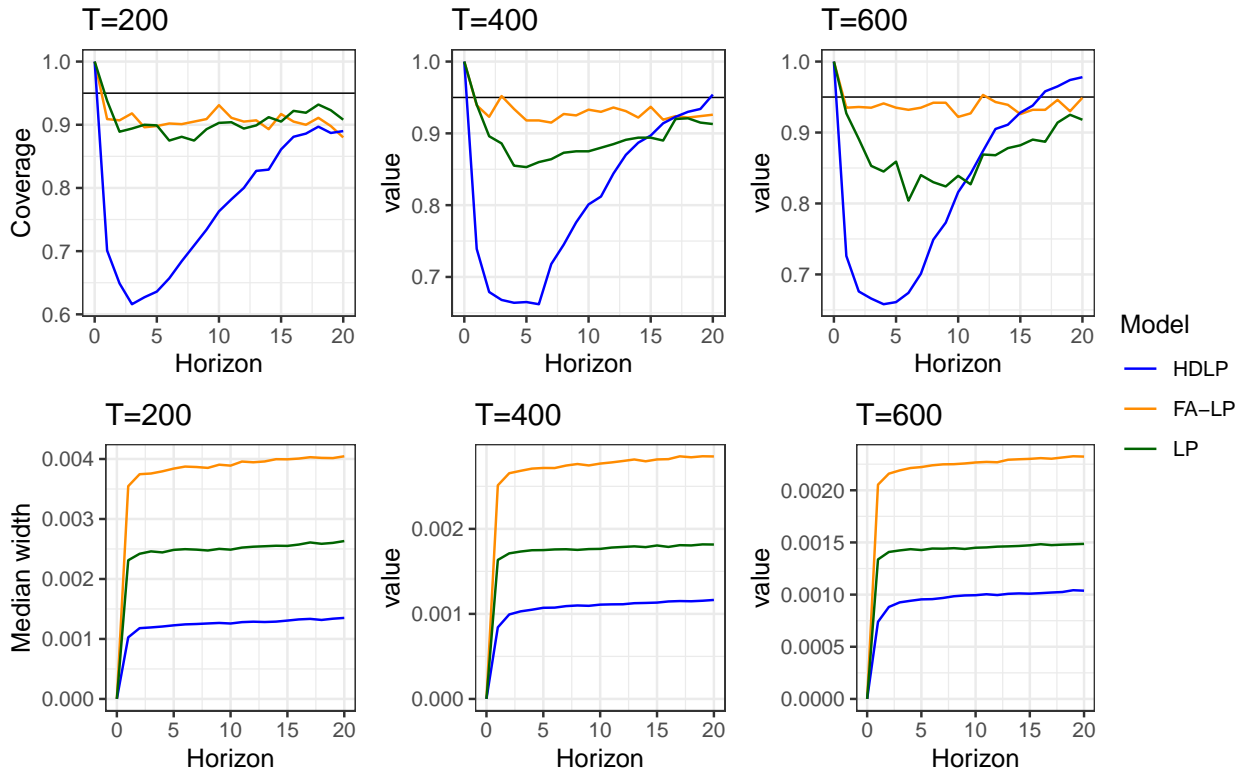


Figure C.4: Coverage rates and median interval widths in the dense DFM.

suggested by Lazarus et al. (2018), namely the (i) Newey-West test “NW-fb” with recommended bandwidth choice  $Q_T = 1.3T^{1/2}$  (Test 2 in Table 1 of Lazarus et al., 2018), and (ii) Equal-weighted cosine test ‘EWC’ with recommended number of cosine terms  $\nu = 0.4T^{2/3}$  (Test 3 in Table 1 of Lazarus et al., 2018). Both estimators are inconsistent, but can be used for valid inference using fixed- $b$  asymptotics. For the former, we use nonstandard critical values tabulated in Table 1 of Kiefer and Vogelsang (2005). For the latter, we use critical values from the  $t_\nu$  distribution. For further details on both estimators, see Section 2 of Lazarus et al. (2018) and references therein. Figure C.5 displays the coverage rates (top panels) and interval widths (bottom panels) for the proposed HDLP method with the three choices of long-run covariance estimator in the dense DFM simulation DGP, Figure C.6 for the sparse DFM.

In the dense DFM, we see that the EWC estimator largely corrects for the poor coverage of the HDLP model with default NW estimator, giving coverage around 90% at horizon 1 and reaching nominal coverage around horizon 15. The NW-fb estimator generally has slightly worse coverage than the default NW, except for the first horizon where both perform similarly. Note that the poor performance of NW-fb compared to NW may appear contradictory with Lazarus et al. (2018), e.g. Table 6 therein. This difference occurs likely due to the fact that we do not use the “textbook NW” estimator of Lazarus et al. (2018) with bandwidth  $Q_T = 0.75T^{1/3}$  but instead the adaptive bandwidth  $Q_T = 1.1447(\hat{\alpha}(1)T)^{1/3}$ , with  $\hat{\alpha}(1)$  computed according to equation (6.4) in Andrews (1991). Looking at the median interval widths, we see that the improved coverage of the EWC comes at the cost of much wider intervals, being approximately 4-6 times as wide as the ones for the default NW across different sample sizes. The NW-fb intervals, in contrast, are slightly tighter, which likely contributes to the poorer coverage.

In the sparse DFM, the EWC estimator achieves the best coverage at nominal rates when

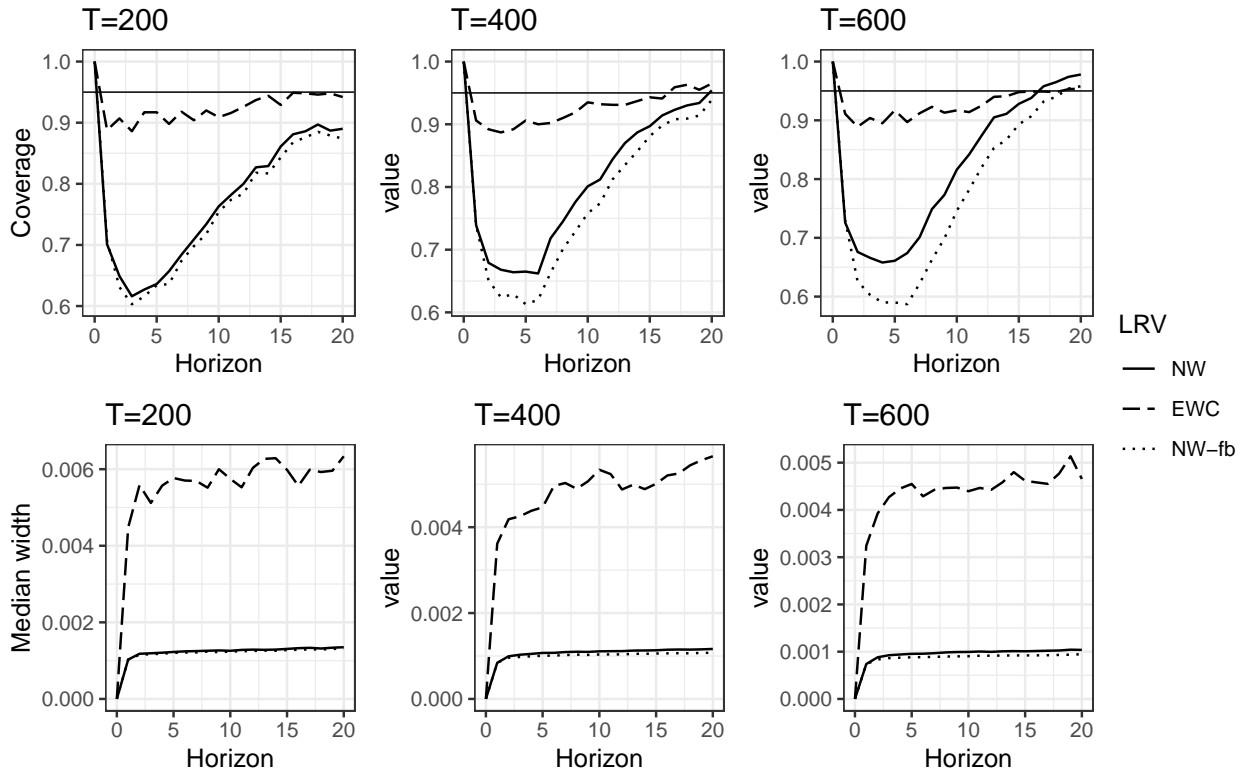


Figure C.5: Coverage rates and median interval widths of HDLP with different long-run covariance estimators in the dense DFM.

$T = 200$ , compared to the regular NW at around 85%. This difference narrows for the larger sample sizes  $T = 400$  and  $600$  where both are slightly conservative in the 95-97% coverage range. The NW-fb estimator performs generally worse than the regular NW. Besides, the relative interval sizes of the three estimators are similar to the ones discussed in the dense DFM simulation design.

Overall, in the dense DFM where we expect the HDLP to suffer, the EWC results in near nominal coverage but comes at a high cost of wide intervals, unlike the NW. In the sparse DFM, the coverage of HDLP with either NW or EWC is more similar—especially at larger sample sizes—but the EWC’s intervals still remain much larger. Additionally, the performance of the NW-fb estimator is generally worse than our adaptive implementation of NW.

## C.2 Data Description

Table C.1: Definition of transformation codes

T	Transformation
1	$f(x_t) = x_t$
2	$f(x_t) = x_t - x_{t-1}$
3	$f(x_t) = (x_t - x_{t-1}) - (x_{t-1} - x_{t-2})$
4	$f(x_t) = \log(x_t)$
5	$f(x_t) = \log(x_t) - \log(x_{t-1})$
6	$f(x_t) = (\log(x_t) - \log(x_{t-1})) - (\log(x_{t-1}) - \log(x_{t-2}))$

In the following tables, the data transformation codes follow the definitions in Table C.1. Codes marked with an asterisk indicate a transformation that is different from the default provided by

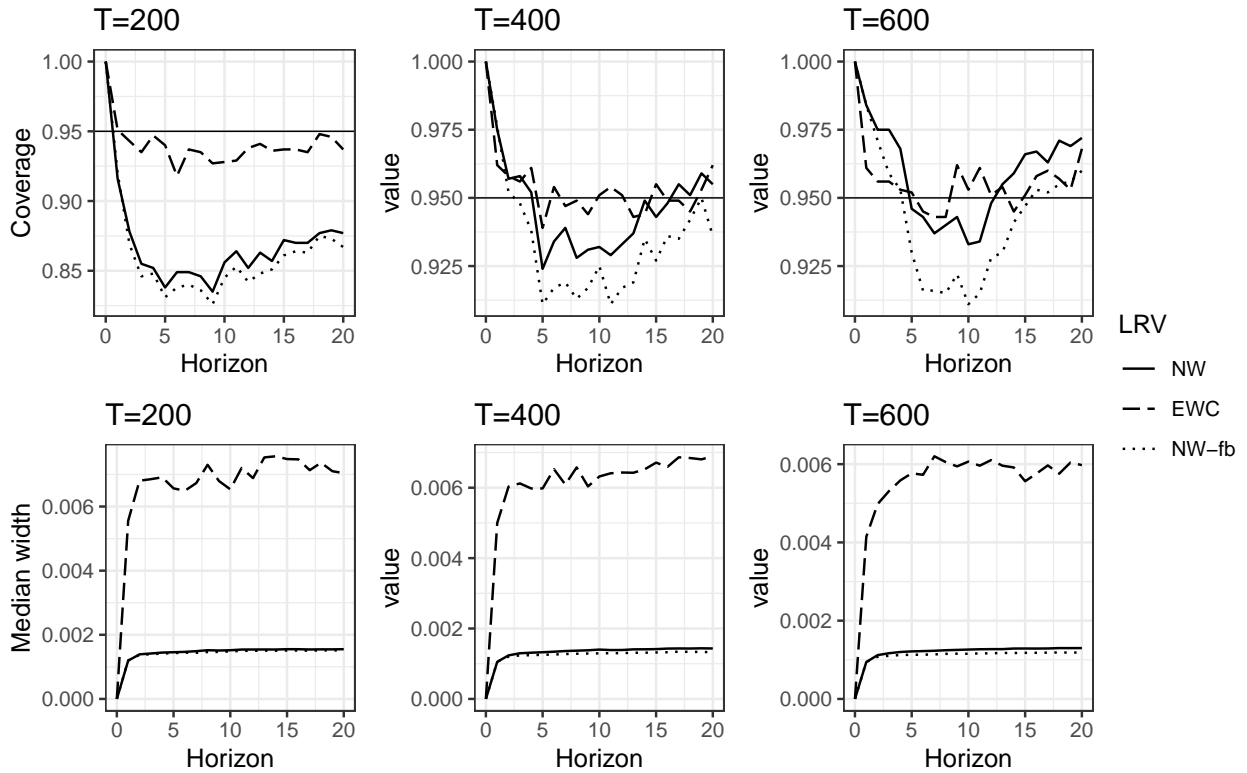


Figure C.6: Coverage rates and median interval widths of HDLP with different long-run covariance estimators in the sparse DFM.

McCracken and Ng (2016b) where we use the transformations in Bernanke et al. (2005) instead. The F/S column indicates whether we treat the variable as fast or slow respectively for our identification scheme.

Table C.2: Output & Income

	FRED	Description	DRI/McGraw	T	F/S
1	RPI	Real Personal Income	GMPYQ	5	S
2	W875RX1	Real personal income ex transfer receipts	GMYXPQ	5	S
3	INDPRO	IP Index	IP	5	S
4	IPFPNSS	IP: Final Products and Nonindustrial Supplies	IPP	5	S
5	IPFINAL	IP: Final Products (Market Group)	IPF	5	S
6	IPCONGD	IP: Consumer Goods	IPC	5	S
7	IPDCONGD	IP: Durable Consumer Goods	IPCD	5	S
8	IPNCONGD	IP: Nondurable Consumer Goods	IPCN	5	S
9	IPBUSEQ	IP: Business Equipment	IPE	5	S
10	IPMAT	IP: Materials	IPM	5	S
11	IPDMAT	IP: Durable Materials	IPMD	5	S
12	IPNMAT	IP: Nondurable Materials	IPMND	5	S
13	IPMANSICS	IP: Manufacturing (SIC)	IPMFG	5	S
14	IPB51222S	IP: Residential Utilities	IPUT	5	S
15	IPFUELS	IP: Fuels	-	5	S
17	CUMFNS	Capacity Utilization: Manufacturing	IPXMCA	1*	S

Table C.3: Money &amp; Credit

	FRED	Description	DRI/McGraw	T	F/S
1	M1SL	M1 Money Stock	FM1	5*	F
2	M2SL	M2 Money Stock	FM2	5*	F
3	M2REAL	Real M2 Money Stock	FM2DQ	5	F
4	BOGMBASE	St. Louis Adjusted Monetary Base	FMFBA	5*	F
5	TOTRESNS	Total Reserves of Depository Institutions	FMRRA	5*	F
6	NONBORRES	Reserves Of Depository Institutions	FMRNBA	5*	F
7	BUSLOANS	Commercial and Industrial Loans	FCLNQ	5*	F
8	REALLN	Real Estate Loans at All Commercial Banks	-	6	F
9	NONREVSL	Total Nonrevolving Credit	CCINRV	5*	F
10	CONSPI	Nonrevolving consumer credit to Personal Income	-	2	F
12	DTCOLNVHFNM	Consumer Motor Vehicle Loans Outstanding	-	6	F
13	DTCTHFNM	Total Consumer Loans and Leases Outstanding	-	6	F
14	INVEST	Securities in Bank Credit at All Commercial Banks	-	6	F

Table C.4: Labour Market

	FRED	Description	DRI/McGraw	T	F/S
1	HWI	Help-Wanted Index for United States	LHEL	5*	S
2	HWIURATIO	Ratio of Help Wanted/No. Unemployed	LHELX	4*	S
3	CLF16OV	Civilian Labor Force	LHEM	5	S
4	CE16OV	Civilian Employment	LHNAG	5	S
5	UNRATE	Civilian Unemployment Rate	LHUR	1*	S
6	UEMPMEAN	Average Duration of Unemployment (Weeks)	LHU680	1*	S
7	UEMPLT5	Civilians Unemployed - Less Than 5 Weeks	LHU5	1*	S
8	UEMP5TO14	Civilians Unemployed for 5-14 Weeks	LHU14	1*	S
9	UEMP15OV	Civilians Unemployed - 15 Weeks & Over	LHU15	1*	S
10	UEMP15T26	Civilians Unemployed for 15-26 Weeks	LHU26	1*	S
11	UEMP27OV	Civilians Unemployed for 27 Weeks and Over	-	5	S
12	CLAIMSx	Initial Claims	-	5	S
13	PAYEMS	All Employees: Total nonfarm	LPNAG	5	S
14	USGOOD	All Employees: Goods-Producing Industries	LPGD	5	S
15	CES1021000001	All Employees: Mining and Logging: Mining	LPMI	5	S
16	USCONS	All Employees: Construction	LPCC	5	S
17	MANEMP	All Employees: Manufacturing	LPEM	5	S
18	DMANEMP	All Employees: Durable goods	LPED	5	S
19	NDMANEMP	All Employees: Nondurable goods	LPEN	5	S
20	SRVPRD	All Employees: Service-Providing Industries	LPSP	5	S
21	USTPU	All Employees: Trade, Transportation & Utilities	LPTU	5	S
22	USWTRADE	All Employees: Wholesale Trade	LPT	5	S
23	USTRADE	All Employees: Retail Trade	-	5	S
24	USFIRE	All Employees: Financial Activities	LPFR	5	S
25	USGOVT	All Employees: Government	LPGOV	5	S
26	CES0600000007	Avg Weekly Hours : Goods-Producing	-	1	S
27	AWOTMAN	Avg Weekly Overtime Hours : Manufacturing	LPMOSA	1*	S
28	AWHMAN	Avg Weekly Hours : Manufacturing	LPHRM	1	S
30	CES0600000008	Avg Hourly Earnings : Goods-Producing	-	6	S
31	CES2000000008	Avg Hourly Earnings : Construction	LEHCC	5*	S
32	CES3000000008	Avg Hourly Earnings : Manufacturing	LEHM	5*	S

Table C.5: Consumption &amp; Orders

	FRED	Description	DRI/McGraw	T	F/S
1	HOUST	Housing Starts: Total New Privately Owned	HSFR	4	F
2	HOUSTNE	Housing Starts, Northeast	HSNE	4	F
3	HOUSTMW	Housing Starts, Midwest	HSMW	4	F
4	HOUSTS	Housing Starts, South	HSSOU	4	F
5	HOUSTW	Housing Starts, West	HSWST	4	F
6	PERMIT	New Private Housing Permits (SAAR)	-	4	F
7	PERMITNE	New Private Housing Permits, Northeast (SAAR)	-	4	F
8	PERMITMW	New Private Housing Permits, Midwest (SAAR)	-	4	F
9	PERMITS	New Private Housing Permits, South (SAAR)	-	4	F
10	PERMITW	New Private Housing Permits, West (SAAR)	-	4	F

Table C.6: Orders &amp; Inventories

	FRED	Description	DRI/McGraw	T	F/S
1	DPCERA3M086SBEA	Real personal consumption expenditures	GMCQ	5	S
2	CMRMTSPLx	Real Manu. and Trade Industries Sales	-	5	F
3	RETAILx	Retail and Food Services Sales	-	5	F
9	AMDMNOx	New Orders for Durable Goods	-	5	F
11	AMDMUOx	Unfilled Orders for Durable Goods	-	5	F
12	BUSINVx	Total Business Inventories	-	5	F
13	ISRATIOx	Total Business: Inventories to Sales Ratio	-	2	F

Table C.7: Interest rate &amp; Exchange rates

	FRED	Description	DRI/McGraw	T	F/S
1	FEDFUNDS	Effective Federal Funds Rate	FYFF	1*	F
2	CP3Mx	3-Month AA Financial Commercial Paper Rate	-	2	F
3	TB3MS	3-Month Treasury Bill	FYGM3	1*	F
4	TB6MS	6-Month Treasury Bill	FYGM6	1*	F
5	GS1	1-Year Treasury Rate	FYGT1	1*	F
6	GS5	5-Year Treasury Rate	FYGT5	1*	F
7	GS10	10-Year Treasury Rate	FYGT10	1*	F
8	AAA	Moody's Seasoned Aaa Corporate Bond Yield	FYAAAC	1*	F
9	BAA	Moody's Seasoned Baa Corporate Bond Yield	FYBAAC	1*	F
10	COMPAPFFx	3-Month Commercial Paper Minus FEDFUNDS	-	1	F
11	TB3SMFFM	3-Month Treasury C Minus FEDFUNDS	SFYGM3	1	F
12	TB6SMFFM	6-Month Treasury C Minus FEDFUNDS	SFYGM6	1	F
13	T1YFFM	1-Year Treasury C Minus FEDFUNDS	SFYGT1	1	F
14	T5YFFM	5-Year Treasury C Minus FEDFUNDS	SFYGT5	1	F
15	T10YFFM	10-Year Treasury C Minus FEDFUNDS	SFYGT10	1	F
16	AAAFFM	Moody's Aaa Corporate Bond Minus FEDFUNDS	SFYAAAC	1	F
17	BAAFFM	Moody's Baa Corporate Bond Minus FEDFUNDS	SFYBAAC	1	F
19	EXSZUSx	Switzerland / U.S. Foreign Exchange Rate	EXRSW	5	F
20	EXJPUSx	Japan / U.S. Foreign Exchange Rate	EXRJAN	5	F
21	EXUSUKx	U.S. / U.K. Foreign Exchange Rate	EXRUK	5	F
22	EXCAUSx	Canada / U.S. Foreign Exchange Rate	EXRCAN	5	F

Table C.8: Prices

	FRED	Description	DRI/McGraw	T	F/S
1	WPSFD49207	PPI: Finished Goods	PWFSA	5*	S
2	WPSFD49502	PPI: Finished Consumer Goods	PWFCSA	5*	S
3	WPSID61	PPI: Intermediate Materials	PWIMSA	5*	S
4	WPSID62	PPI: Crude Materials	PWCMSA	5*	S
5	OILPRICE <sub>x</sub>	Crude Oil, spliced WTI and Cushing	-	6	F
6	PPICMM	PPI: Metals and metal products	-	6	S
8	CPIAUCSL	CPI : All Items	PUNEW	5*	S
9	CPIAPPSL	CPI : Apparel	PU83	5*	S
10	CPITRNSL	CPI : Transportation	PU84	5*	S
11	CPIMEDSL	CPI : Medical Care	PU85	5*	S
12	CUSR0000SAC	CPI : Commodities	PUC	5*	S
13	CUSR0000SAD	CPI : Durables	PUCD	5*	S
14	CUSR0000SAS	CPI : Services	PUS	5*	S
15	CPIULFSL	CPI : All Items Less Food	PUXF	5*	S
16	CUSR0000SA0L2	CPI : All items less shelter	PUXHS	5*	S
17	CUSR0000SA0L5	CPI : All items less medical care	PUXM	5*	S
18	PCEPI	Personal Cons. Expend.: Chain Index	-	6	S
19	DDURRG3M086SBEA	Personal Cons. Exp: Durable goods	GMCDQ	5*	S
20	DNDGRG3M086SBEA	Personal Cons. Exp: Nondurable goods	GMCNQ	5*	S
21	DSERRG3M086SBEA	Personal Cons. Exp: Services	GMCSQ	5*	S

Table C.9: Stock Market

	FRED	Description	DRI/McGraw	T	F/S
1	S&P 500	S&P's Common Stock Price Index: Composite	FSPCOM	5	F
2	S&P: indust	S&P's Common Stock Price Index: Industrials	FSPIN	5	F
3	S&P div yield	S&P's Composite Common Stock: Dividend Yield	FSDXP	1*	F
4	S&P PE ratio	S&P's Composite Common Stock: Price-Earnings Ratio	FSPXE	1*	F

### C.3 FAVAR Implementation

We closely follow the method described in Bernanke et al. (2005) to estimate the FAVAR. The most important difference concerns the scaling of all impulse responses by the response of the FFR at horizon 0. That means the shock to which the variables are responding is of such a size that the FFR rises by one on impact, as opposed to a size of one standard deviation, as is done by Bernanke et al. (2005). We implement this change to ensure that the scale of the responses from the FAVAR are comparable to those from our HDLP specification.

Let  $\mathbf{X}_{\text{all}}$  denote the matrix containing all variables, and  $\mathbf{X}_{\text{slow}}$  the one containing only the “slow” variables which we assume to not react within the same period to a monetary policy shock. We then estimate the factors  $\hat{\mathbf{C}}$  and  $\hat{\mathbf{C}}^*$  as the first 3 principal components of  $\mathbf{X}_{\text{all}}$  and  $\mathbf{X}_{\text{slow}}$  respectively. We regress  $\hat{\mathbf{C}}$  onto  $\hat{\mathbf{C}}^*$  and  $\mathbf{R}_s$ , where  $\mathbf{R}_s$  is the FFR ( $\mathbf{R}$ ) scaled such that it has mean 0 and variance 1, and estimate by OLS

$$\hat{\mathbf{C}} = \begin{bmatrix} \hat{\mathbf{C}}^* & \mathbf{R}_s \end{bmatrix} \hat{\boldsymbol{\beta}} + \hat{\mathbf{u}}.$$

We then take  $\hat{\mathbf{b}}_R$  as the last row of  $\hat{\boldsymbol{\beta}}$ , and let  $\hat{\mathbf{F}} = \hat{\mathbf{C}} - \mathbf{R}_s \hat{\mathbf{b}}_R$ . Next, we use the `vars` package in R to estimate a 13 lag VAR with the four variables in  $[\hat{\mathbf{F}}, \mathbf{R}]$  (ordering the FFR last), and obtain the impulse responses of the factors and  $\mathbf{R}$  using a recursive identification scheme with Cholesky decomposition, and store them in a matrix  $\mathbf{IR}_{\text{fac}}$ . These impulse responses are all scaled such that we use the unit shock identification, similar to that of local projections. To obtain the impulse responses of the individual variables in  $\mathbf{X}_{\text{all}}$ , we regress  $\mathbf{X}_{\text{all}}$  onto  $\hat{\mathbf{F}}$ , and estimate by OLS

$$\mathbf{X}_{\text{all}} = \hat{\mathbf{F}} \hat{\boldsymbol{\Lambda}} + \hat{\mathbf{v}}.$$

The matrix of impulse responses for all variables is then obtained by

$$\mathbf{IR}_{(h_{\text{max}}+1) \times 122} = \mathbf{IR}_{\text{fac}} \begin{bmatrix} \hat{\boldsymbol{\Lambda}} \\ \mathbf{0} \end{bmatrix}.$$

Finally, we cumulate the impulse responses for the variables which were taken in differences to obtain the response of the level variable.

For inference, we use a simple residual bootstrap. We draw with replacement from the VAR residuals, and use them to construct the bootstrap series  $\hat{\mathbf{F}}^*$  and  $\mathbf{R}^*$ . We then perform the same steps, i.e. estimate the VAR on the bootstrap data, obtain (unit-shock scaled) impulse responses for the factors, compute the (cumulated) implied impulse responses of all variables. We repeat this process  $B = 499$  times and use the 2.5% and 97.5% quantiles to construct confidence intervals.